MAGNETIC AND GRAVITY STUDIES OF BURIED VOLCANIC CENTERS IN THE AMARGOSA DESERT AND CRATER FLAT, SOUTHWEST NEVADA

By
V.E. Langenheim

1995

Open-File Report 95-564

Menlo Park, California
1995

CONTENTS

ILLUSTRATIONS

ABSTRACT

Several dipolar aeromagnetic anomalies occur over flat, alluvium-covered areas of the Amargosa Desert and Crater Flat that resemble anomalies typically associated with subaerial basaltic volcanic centers. Ground magnetic and gravity data were collected over three of these aeromagnetic anomalies near Yucca Mountain, a potential site for long-term storage of high-level radioactive waste. The ground magnetic data suggest the sources of these anomalies are shallowly buried. The lack of a large associated gravity anomaly with the ground magnetic anomalies suggests that either the source rocks may be tuff rather than basalt, or that the volume of the body is small. The latter possibility is more likely because basalt has been found in drillholes located over two Amargosa Desert aeromagnetic anomalies. A map showing optimal locations for proposed drilling of the anomalies based on magnetic modeling is shown. Modeled depths to the top of the sources of these buried anomalies are less than 300 m.

INTRODUCTION

Volcanic hazard studies of the Nevada Test Site are necessary to evaluate the probability of potential volcanism and to predict the effect of such volcanism on the potential nuclear waste repository at Yucca Mountain (Fig. 1). Based on studies of the timing and volumes of eruptions of known volcanic centers in the southern Great Basin, Crowe and others (1982) calculated an annual probability of a volcanic event between 4.7×10^{-8} and 3.3×10^{-10} for the Yucca Mountain area. They stated that the actual probability may be less, based on an observed decrease in erupted volume during the past 4 Ma. If other Pliocene or Quaternary volcanic centers are found, the probability estimates could change significantly (B.M. Crowe, oral commun., 1986). Because of the generally high magnetizations of igneous rocks, magnetic surveys can help locate previously undiscovered buried volcanic centers.

Aeromagnetic surveys of the Lathrop Wells and Timber Mountain areas (U.S. Geological Survey, 1978, 1979; Langenheim and others, 1991) show at least six dipolar anomalies (both normal and reversed polarity) over the flat, alluvial areas of the Amargosa Desert and Crater Flat (Fig. 2). These anomalies are not located near exposed volcanic deposits, but are similar in shape to anomalies associated with subaerial basaltic volcanic centers. For example, the anomaly labeled LW on Figure 1 is associated with the Lathrop

Wells volcanic center, whereas anomalies A through F are not located over exposed volcanic rocks. It therefore seemed likely that basaltic volcanic rocks were buried at locations A through F. In order to locate and characterize the sources of the aeromagnetic anomalies in Amargosa Desert and Crater Flat, ground magnetic and gravity data were collected along profiles over anomalies C, D, and F (Fig. 2).

ACKNOWLEDGMENTS

GEOLOGIC SETTING

The area of interest lies along the southern margin of the southwest Nevada volcanic field which produced voluminous and widespread ash-flow sheets from more than six major calderas >15 to 7.5 Ma (Sawyer and others, 1994) and within the Walker Lane belt (Carr, 1984). The Walker Lane belt is a northwest-trending zone of diverse topography and structure that has undergone substantial lateral shear. Crater Flat is an elliptical basin within the Walker Lane belt, cradled between Yucca Mountain and Bare Mountain. Gravity and seismic refraction data indicate that the basin fill consisting of alluvial deposits and Tertiary volcanic rocks reaches thicknesses of 3 to 4 km (Snyder and Carr, 1984; Mooney and Schapper, 1995). Within Crater Flat, Pliocene cinder cones (1.0 Ma) and basalt flows (3.7 Ma) form a general north-northeast alignment. Miocene (10.5 Ma) basalt and a Quaternary cinder cone (Lathrop Wells, 120 ka; R. Fleck, U.S. Geological Survey, written commun., 1995) are exposed along the southern rim of Crater Flat.

Both Crater Flat and the Amargosa Desert lie within the north-trending structural trough called the Kawich-Greenwater rift. This tectono-volcanic rift represents a pull-apart or stepped zone of rifting within the larger Walker Lane belt and is near and parallel to a zone of Pliocene and Quaternary volcanism called the Death Valley-Pancake Range basalt belt (Carr, 1984). Gravity data (Healey and Miller, 1965) indicate a series of complex northwest- and northeast-trending sub-basins below the flat, alluvial surface of the Amargosa Desert within the rift. Wright (1989) suggests that these basins

2

were caused by pull-apart activity before the eruption of the Paintbrush Group (12.7 Ma; Sawyer and others, 1994). However, Carr (1984) argues that the development of the alluvial basins in this region began about 10 Ma.

PREVIOUS WORK

Langenheim and others (1993) modeled ground magnetic data collected over anomaly B (Fig. 2; anomaly 10 of Kane and Bracken, 1983), the largest of the dipolar aeromagnetic anomalies. The modeling indicated that the depth to the source of the anomaly was less than 250 m and probably less than 150 m. Drilling by an oil company found 50 m of basalt at a depth of 105 m (Duane Champion, 1993, U.S. Geological Survey, written commun.), confirming the magnetic modeling results. Langenheim and others (1993) also presented gravity data collected over a north-south line over the aeromagnetic anomaly. They argue that the lack of a large associated gravity anomaly suggests that either (1) the source of the aeromagnetic anomaly has about the same density as the surrounding alluvium (e.g. it may be composed of tuff) or (2) that the volume of the volcanic center is small. Drillhole data argue for the second alternative that the volume of the center is relatively small. Modeling of the anomaly by Langenheim and Ponce (1993) suggests that the volume of the source of anomaly B is 10 to 40 x 10^7 m^3, consistent with total magmatic volume estimates made by Crowe and others (1983) for other basaltic volcanic centers exposed in Crater Flat (10 x 10^7 m^3 for Black Cone; 2.6 x 10^7 m^3 for Red Cone). Langenheim and Ponce (1993) also presented preliminary volume estimates of the sources of anomalies C, D, and E (1 to 5 x 10^7 m^3) based on calculations of "excess mass" of the pseudogravity transformation of the aeromagnetic anomalies.

Other geophysical studies in the area include seismic refraction profiles carried out in the Amargosa Valley (Mooney and Schapper, 1995). The profiles do not intersect fully any of the aeromagnetic anomalies in Amargosa Desert. The Fortymile Wash profile does image an anomalous feature in the vicinity of anomaly B, but this feature seems to be too deep (500 m) and too large to be the causative body of Anomaly B. This higher-velocity feature protruding into the alluvium may nonetheless be the magma source for anomaly B or could reflect a shallowing of the Paleozoic basement as suggested by an east-northeast ridge of higher gravity values (Fig. 3) and by

3

resistivity data (Greenhaus and Zablocki, 1982) in this area. An east-west seismic reflection profile (coincident with the Amargosa Valley seismic refraction profile) crosses the southernmost tip of anomaly B, but no reflectors in this area were interpreted to be caused by buried basalt (Brocher and others, 1993). A strong reflector (Brocher's reflector "C") is imaged in approximately the same location as the aeromagnetic anomaly, but upon closer inspection, it is 1 to 2 km west of the aeromagnetic anomaly and probably too deep (200 m instead of 100 m) to be caused by the source of Anomaly B.

MAGNETIC AND GRAVITY DATA

119 gravity stations in the Amargosa Desert region and 30 stations in the Crater Flat area were collected . Gravity data were collected along the east-west profile in Crater Flat and along sections of 10 profiles in Amargosa Valley (C1 through C4, C7, and D1 through D5; Fig.s 1 and 3). Gravity stations were spaced about 500 m apart along the traverses. Horizontal and vertical control of each gravity station along the profiles were established using an electronic-distance-measurement instrument and station elevations are accurate to about 0.03 m from a reference benchmark.

Observed gravity data were tied to base station MERC, at the U.S. Geological Survey Core Library building at Mercury, Nevada (Ponce and Oliver, 1981, p. 13). Because of building construction near base station MERC, Ponce and others (1993) determined a new value of 979,518.91 mGal for this station; that new value was used to reduce the data presented in this report. Gravity data were reduced using the Geodetic Reference System of 1967 (International Union of Geodesy and Geophysics, 1971) and referenced to the International Gravity Standardization Net 1971 gravity datum (Morelli, 1974, p. 18). Gravity data were reduced to complete Bouguer anomalies using a reduction density of $2.67 \, g/cm^3$ and include earth-tide, instrument drift, free-air, Bouguer, latitude, earth-curvature, and terrain corrections. Terrain corrections were computed to a radial distance of 167 km and involved a three-part process: (1) Hayford-Bowie zones A and B with an outer radius of 68 m were estimated in the field with the aid of tables and charts, or sketched and later calculated in the office, (2) Hayford-Bowie zones C and D with an outer radius of 590 m were calculated by averaging compartment elevations

on a circular template based on Hayford's system of zones (Swick, 1942, p. 66), and (3) terrain corrections from a distance of 0.59 km to 167 km were calculated using a digital elevation model and a procedure by Plouff (1977). Observed gravity values are accurate to about 0.05 mGal, while Bouguer gravity anomalies are accurate to about 0.1 mGal. Profiles of gravity data are shown in figures 4, 5, and 6.

Ground magnetic data with the sensor at 2.4 m above the surface were collected along 10 profiles in Amargosa Desert (C1 through C5, C7, and D1 through D4) and two profiles in Crater Flat (F1 and F2; Figs. 1 and 2). Ground magnetic data could not be collected along line D5 because of its proximity to a powerline along the entire length of the profile. Locations of magnetic stations between surveyed gravity stations were determined by interpolation using the number of paces and the surveyed distances between the gravity stations. Maximum station spacing was 20 paces or about 18 m, except along stretches of profiles C4 and C7. Minimum spacing was 1 pace or about 1 m.

A model G-816 Geometrics portable proton precession magnetometer and G-826A base station magnetometer were used to collect data. Because the anomalies of interest were believed to be small (20 to 50 nT) and the profile lines were long (up to 4.5 km), a base station magnetometer was used or a temporary base along the traverse was periodically reoccupied during the survey to make corrections for diurnal variations of the Earth's magnetic field. The magnetic measurements were corrected for diurnal variations and are total magnetic field values. Magnetic observations are accurate to about 1 nT. The profiles of the magnetic data are shown in figures 4, 5 and 6.

ANOMALIES C, D, AND F

Anomaly C (Fig. 2) is located about 15 km southwest of the town of Amargosa Valley (formerly called Lathrop Wells). Anomaly C is dipolar with its magnetic low on the south side, indicating that the magnetization of the source body is reversed. It has an amplitude of 350 nanoteslas (nT) measured at 122 meters above the alluvial surface (U.S. Geological Survey, 1978; Langenheim and others, 1991). The maximum amplitude of the anomaly

5

measured 2.44 m (8 ft) above the ground is about 600 nT along profile C5 (Fig. 4e). If we assume that the source of the anomaly is a narrow, vertically oriented magnetic monopole (such as a magnetic dike), we can relate the ground and aeromagnetic field measurements, F_1 and F_2, to the distances of the source to the height of measurement, r_1 and r_2, using the following equation:

$$F_1/F_2 = (r_2/r_1)^2,$$

where r_2 equals r_1 +120 m. Using the above equation, the predicted depth to the top of the body is about 390 m. The actual depth to the top of the body may be shallower or deeper, depending on the geometry of the source. Along profile C2 (Fig. 4b), an east-west traverse across the southern low of the anomaly, the anomaly is roughly 2.5 km wide and consists of two lows about 1 km apart. Gravity data collected along C2 indicate a 1-mGal high centered on the ridge between the two magnetic lows. Gravity highs of 1 mGal or less roughly coincide with the ground magnetic expression of Anomaly C along profiles C1, C3, and C4. Although no detailed gravity data were collected along profile C5, gridded gravity values indicate a 1-mGal-high at the location of the ground magnetic high (Fig. 4e).

Anomaly D is located about 4 km southeast of anomaly C (Fig. 2). In contrast to anomaly C, the magnetic signature of anomaly D indicates that the source of the anomaly is normally polarized. Its aeromagnetic anomaly has an amplitude of about 300 nT. Its ground magnetic anomaly has a double-peaked high along profile D1 (Fig. 5a) with a maximum amplitude of about 850 nT along profile D4 (Fig. 5d). Using the ratio of field measurements and distances, the predicted depth to the top of the body is about 175 m. Magnetic data along D2 (Fig. 5b), an east-west profile, indicate that Anomaly D is about 1 km wide. Background magnetic values along D2 have amplitudes of 25 nT or less. A gravity high of about 0.7 to 0.8 mGal coincides with the location of the magnetic high on profiles D2 and D3 (Fig. 5c). A 3-mGal high roughly coincides with the location of Anomaly D along profile D1; however, the breadth and amplitude of the anomaly suggests that the gravity high is also partly caused by topography on the Paleozoic bedrock surface. Along profile D5 (Fig. 5e) crossing the southern edge of the aeromagnetic high, little to no expression (< 0.3 mGal) of Anomaly D exists in the gravity field. About 9 m

(30 feet) of basalt were found at the bottom of a 190-m deep drillhole near Anomaly D (Walker and Eakin, 1963). The presence of basalt at this location strongly suggests that the source of the aeromagnetic and ground magnetic anomalies is basalt.

Anomaly F (Fig. 2; anomaly 26 of Kane and Bracken, 1983) is located about 2 km south of Little Cones in Crater Flat. Its amplitude at a height of 122 meters above the ground surface is about 400 nT. Its ground magnetic amplitude along F2 (Fig. 6b) is almost 1000 nT. Using the ratio of field measurements and distances, the predicted depth to the top of the body is about 206 m. Like Anomaly D, the anomaly is normally polarized. Its prominent magnetic high interrupts the trough of low aeromagnetic field values along the west side of Crater Flat (Fig. 2). Ground magnetic data along F1 indicate two magnetic highs with amplitudes of 200 and 800 nT; the width of the ground magnetic anomaly is about 2 km. A small gravity anomaly with a maximum amplitude of about 1 mGal interrupts the steep gravity gradient along F1 and coincides with the location of the larger ground magnetic peak (Fig. 6a). Although no detailed gravity data were collected along profile F2, gridded gravity values indicate a 1-mGal-high superimposed on the gravity gradient in the vicinity of the ground magnetic anomaly (Fig. 6b). Wildly fluctuating ground magnetic values along the northern 350 m of profile F2 reflect highly magnetic basaltic float derived from Little Cones. The sharp magnetic low at the southern end of the profile is probably caused by exposed and very shallowly buried volcanic deposits located just south of the terminus of the profile.

MODELING

The goal of modeling the ground magnetic data is to estimate the maximum depth to the top of the causative body and to locate the edges of the causative body. A map showing the locations of the optimal places to drill the sources of the anomalies based on the models (Figures 7, 8, and 9) is shown on Figure 10. Two locations are shown for Anomaly D because of the double-peaked ground magnetic high observed along profile D1. This information will be useful for future drilling of the body.

Modeling of the ground magnetic anomalies is ambiguous because of the

lack of information on the magnetic properties of the buried bodies. Magnetic properties of lava flows at the Nevada Test Site are highly variable and can only be reliably determined by sampling (Bath, 1967). Nonetheless, the sharp gradients defining these magnetic anomalies indicate that the anomalies are probably caused by strongly magnetized rocks at shallow depth (less than 1 km) and previous modeling of anomaly B, based on the following assumptions about the magnetic properties of the causative source, was successful in predicting the depth to the top of the basalt.

For these 2-1/2-dimensional models, the causative body is assumed to be basalt, based on the drilling results for anomalies B and D. An intensity of magnetization of 0.01 emu/cm^3 for the causative body is assumed for all the models. This assumption is based on preliminary natural remanent magnetization measurements on the 1.0 Ma cinder cones in Crater Flat and basaltic chips from the drillhole that penetrated the source of Anomaly B (Duane Champion, U.S. Geological Survey, oral commun., 1991). The true intensity of magnetization may be as little as one-fifth of that used in the models if the causative body is tuff or weakly magnetized basalt. If the intensity of magnetization were doubled, the thickness of the modelled body would decrease by about half or the body could be somewhat deeper. Induced magnetization may contribute to the overall magnetization of the body, although the reversed polarity of anomaly C indicates that the remanent magnetization is several times larger than the induced magnetization of the source rocks.

The polarity of the anomaly was used to help estimate the direction of remanent magnetization. For anomaly C, a reversely-polarized anomaly, the assumed direction of remanent magnetization has an inclination of -55° and a declination of 180°. For the normally polarized anomalies D and F, the direction of remanent magnetization has an inclination of 55° and a declination of 0°. These assumptions are based on the direction of magnetization expected for the latitude of Amargosa Desert and Crater Flat from the dipole model of the geomagnetic field (McElhinny, 1973); the assumed directions are consistent with directions measured on the 1.0 Ma and 3.7 Ma basalts in Crater Flat (Champion, 1991). The uncertainty in the assumed direction of magnetization is probably 20° based on studies of secular

variation. A change of 20° in declination and inclination does not significantly affect the models. For example, a steeper inclination (70°) would give a better fit to the northern low of the model of Anomaly D (Fig. 8) without significantly affecting the depth estimate or location of the source. An additional body was added to the model of Anomaly F (Fig. 9) to approximate the effects of basalt associated with the Little Cones volcanic center, using a declination of 178° and an inclination of -64° (Champion, 1991) and an intensity of magnetization of 0.01 emu/cm^3.

Modeling along the north-south profile C5 indicates an estimated maximum depth of 200 m to the top of the causative body (Fig. 7). Typical basalt flows have sides with shallower dips than the one shown in Figure 7; this geometry would cause the source to be even shallower and thinner in order to match the observed gradients of the anomaly. Although gravity data were not collected along C5, forward modeling of the body indicates a maximum gravity anomaly of 1.2 mGal, using a density contrast of 0.8 g/cm^3. This value agrees well with the anomaly observed in gridded gravity data. The gravity anomaly observed along profile C1 (Fig. 4a) is consistent in both magnitude and wavelength with the forward model. Gravity anomalies coincident with the ground magnetic anomalies on profiles C2 (Fig. 4b) and C4 (Fig. 4d) are somewhat larger in magnitude and broader than the proposed anomaly along C5. However, the ground magnetic anomaly observed on C2 is broader than that observed on C5; thus, the gravity anomaly along C2 should be broader than that along C5. The observed gravity anomaly along profile C3 (Fig. 4c) is somewhat smaller, about 0.3 mGal.

Modeling along profile D1 indicates a depth of 180 m to the top of the causative body of Anomaly D (Fig. 8). This result is consistent with the depth of basalt (190 m; Walker and Eakin, 1963) found in a drillhole just west of the maximum amplitude of the anomaly. If the assumed properties of the body are correct, the thickness of the body is about 70 m. The double-peaked anomaly suggests either (1) topography on the top surface of the causative body, (2) variations of the magnetic properties within a single causative body, or (3) the presence of two volcanic vents separated by about 600 to 700 m. Topography on the top surface of the body may have resulted from erosion or faulting. Anomaly D is less than 1 km south of the Rock Valley Wash fault

9

zone (Swadley, 1983); movement along this fault system is as recent as Quaternary and could certainly have affected the source of anomaly D. Bath (1967) and Rosenbaum and Snyder (1985) have documented large variations in the magnetic properties of volcanic rocks at the Nevada Test Site and Yucca Mountain. Forward gravity modeling along D1 suggests that the resulting gravity anomaly of a body with topography on its top surface will also be double-peaked, but asymmetric, with a maximum amplitude of 1.3 mGal. However, the magnitude of the gravity low between the gravity peaks is only about 0.1 to 0.2 mGal, which is the resolution of the data. In addition, the observed gravity anomaly along D1 (about 3 mGal) appears to be dominated by larger-scale features related to topography on the Paleozoic basement surface (Fig. 3). Gravity data along other profiles across anomaly D do show anomalies of 0.2 to 0.6 mGal in the same location of the ground magnetic anomalies.

Modeling of the north-south profile across anomaly F indicates a depth of about 200 m to the top of the causative body (shaded body, Fig. 9) and a thickness of about 100 m. If the body has vertical sides, the depth to the top of the body is about 300 m (dashed body, Fig. 9). Although gravity data were not collected along profile F2, forward gravity modeling of the shaded body in Figure 9 indicates a maximum anomaly of 1.3 mGal. Gravity data were collected along profile F1 (Fig. 6a) and are dominated by a steep gradient caused by the juxtaposition of high-density, Precambrian and Paleozoic rocks exposed at Bare Mountain and the thick alluvial deposits and low-density volcanic rocks of Crater Flat along the Bare Mountain fault. However, a 1-mGal anomaly interrupts the smooth, steep gravity gradient in the same location as the ground magnetic anomaly and may reflect the source of anomaly F, rather than a step in the Bare Mountain fault. A similar 1-mGal gravity high is observed in gridded gravity data along profile F2.

An evenly spaced grid of gravity data may help further constrain the shape and size of the causative bodies of anomalies C, D, and F. A large density contrast is expected between basalt and alluvium (0.4 to 0.8 g/cm^3), and the apparent lack of an associated gravity anomaly suggests that either the causative body may be tuff rather than basalt, or the volume of the body is small. Because basalt is found in drillholes in the areas of anomalies B and D,

the volumes of the buried basalts in these areas must be small.

DISCUSSION

The age and composition of the bodies can only be determined by sampling, although some inferences can be made from the magnetic and gravity modeling results. Crowe (1986) divides basalts in the Death Valley-Pancake Range volcanic zone into two major types of volcanic fields based on volume, composition, and longevity. Type-I volcanic fields are large-volume (> 2000 x 10^7 m^3), long-lived fields characterized by a range in basalt types and by associated silicic rocks that were derived from fractionation of the basaltic magmas or produced by melting of the lower crust. Type-II volcanic fields are short-lived and are characterized by small volumes (generally < 100 x 10^7 m^3) and evolved basaltic magmas ("hawaiities"). Because the gravity and magnetic data indicate that the sources of the magnetic anomalies have small volumes, the sources of Anomalies C, D, and F most likely belong to Crowe's type-II volcanic field and, thus, probably are characterized by hawaiite compositions.

An electrical resistivity study of the Amargosa Desert (Greenhaus and Zablocki, 1982) shows that the depth to resistive Paleozoic basement rocks near Anomaly C is approximately 800 m. Gravity data inverted for thickness of Cenozoic deposits suggest that the depth to Paleozoic rocks is even deeper, ranging from 1000 to 1500 m (Jachens and Moring, 1990; Langenheim and Ponce, 1995). These depths are significantly deeper than the estimated maximum depth to the top of the source from magnetic modeling, suggesting that the causative body is embedded in the alluvial deposits. If the body is a cinder cone, it apparently did not erupt on a former Paleozoic surface and has been completely buried. Like Anomaly C, electrical resistivity and gravity data indicate that the source of Anomaly D is embedded in alluvial deposits. Thus, the sources of these anomalies must be Miocene or younger.

Gravity data indicate that the depth to Paleozoic rocks in the area of anomaly F is about 700 to 1000 m (Jachens and Moring, 1990; Langenheim and Ponce, 1995), suggesting that the source of Anomaly F is also embedded in Cenozoic deposits. Another possible constraint on the age of Anomaly F's source is the presence of 10.5 Ma reversely magnetized basalt at a depth of 360

m in drillhole VH-2 (located about 1.5 km north of Red Cone; Carr and Parrish, 1985). Aeromagnetic data suggest that this basalt is continuous along the west side of Crater Flat and is contiguous with basaltic outcrops along the southwest margin of Crater Flat. Thus, the aeromagnetic data suggest that 10.5 Ma basalt is buried in the area of Anomaly F, presumably at depths of 350 to 400 m. Magnetic modeling suggests that the normally polarized source of anomaly F lies stratigraphically above the reversely magnetized basalt; thus, it would be younger than 10.5 Ma.

The sense of polarity of the anomalies may help constrain the ages of the sources and establish relative ages of the sources. For example, if the causative body of Anomaly C is basalt, its reversed polarity suggests that the body formed during one of three known periods of reversely polarized basaltic volcanism recognized in the Crater Flat area, 10.5, 3.7, and 1.0 Ma. However, the reversed polarity of Anomaly C does not restrict its age to those three periods. Dating of basalt chips from a drillhole that penetrated the source of Anomaly B, another reversely-polarized anomaly in the Amargosa Desert, indicates that the basalt flow may be 4.4 Ma instead of 3.7 Ma (Crowe and others, 1995). Using an average rate of burial based on the age and depth of burial of the Anomaly B basalt of 0.03 mm/yr (consistent with the average rate of sedimentation in Crater Flat during the last 10 to 11 Ma; Carr, 1984), the estimated maximum age of Anomaly C is about 6.7 Ma, assuming it was buried quickly.

Regardless of the age of Anomaly C, the ages of the sources of Anomalies D and F must be different from that of Anomaly C because of their normal polarity. Normally polarized basaltic volcanism in the vicinity of Crater Flat and Amargosa Valley includes the Lathrop Wells cone (120 ka), Sleeping Buttes (340 ka), and Buckboard Mesa (2.9 Ma). However, it is unlikely that the buried sources of these anomalies, D and F, belong to any of these young episodes of normally polarized volcanism. Assuming an average rate of burial of 0.03 mm/yr, the age of basalt found at a depth of 190 m in the area of Anomaly D is about 6.3 Ma. According to this method, the maximum age of Anomaly F is 10 Ma, but is probably much younger based on the magnetic model of a geologically more reasonable geometry of the source rocks (shaded body in Fig. 9).

CONCLUSION

Modeling of anomalies C, D, and F indicates that the estimated maximum depth to the top of the causative bodies is less than 300 m. The modeling also helps pinpoint locations for proposed drilling of the anomalies (Fig. 10). Although it is not possible to determine uniquely the geometry and volume of the magnetic sources of Anomalies C, D, and F, drilling along with additional gravity and magnetic data, should yield significant information on the nature of the volcanism that produced these anomalies. In addition, gravity and ground magnetic data are needed to characterize anomalies A and E in the Amargosa Desert. Modeling of the aeromagnetic anomalies over alluvial areas near the potential Yucca Mountain high-level waste site can contribute to a better understanding of the history of volcanism in the area as well as supplement volume estimates necessary for calculating the probability of future volcanism at Yucca Mountain.

REFERENCES CITED

Bath, G.D., 1967, Aeromagnetic anomalies related to remnant magnetism in volcanic rocks, Nevada Test Site: U.S. Geological Survey Open-File Report 973, 20 p.

Brocher, T.M., Carr, M.D., Fox, K.F., Jr., and Hart, P.E., 1993, Seismic reflection profiling across Tertiary extensional structures in the eastern Amargosa Desert, southern Nevada, Basin and Range province: Geological Society of America Bulletin, v. 105, p. 30-46.

Carr, W.J., 1984, Regional structural setting of Yucca Mountain, southwestern Nevada, and late Cenozoic rates of tectonic activity in part of the southwestern Great Basin, Nevada and California: U.S. Geological Survey Open-File Report 84-854, 109 p.

Carr, W.J., and Parrish, L.D., 1985, Geology of drillhole USW VH-2, and structure of Crater Flat, southwestern Nevada: U.S. Geological Survey Open-File Report 85-475, 41 p.

Champion, D.E., 1991, Volcanic episodes near Yucca Mountain as determined by paleomagnetic studies at Lathrop Wells, Crater Flat, and Sleeping Butte, Nevada: Proceedings, High Level Radioactive Waste Management Conference, American Nuclear Society, p. 61-67.

Crowe, B.M., 1986, Volcanic hazard assessment for disposal of high-level radioactive waste, (Chap. 16) *in* Active Tectonics: Impact on Society: National Academy Press, Washington, D.C., p. 247-260.

Crowe, B.M., Johnson, M.E. and Beckman, R.J., 1982, Calculation of the probability of volcanic disruption of a high-level radioactive waste repository within southern Nevada: Radioactive Waste Management and the Nuclear Fuel Cycle, v. 3, p. 167-190.

Crowe, B.M., Vaniman, D.T., and Carr, W.J., 1983, Status of volcanic hazard studies for the Nevada nuclear waste storage investigations: Los Alamos National Laboratory report LA-9325-MS, 46 p., 1 plate, scale 1:1,000,000.

Crowe, B.M., Perry, F., Geissman, J., McFadden, L., Wells, S., Murrell, M., Poths, J., Valentine, G.A., Bowker, L., and Finnegan, K., 1995, Status of volcanism studies for the Yucca Mountain site characterization project: Los Alamos National Laboratory Report LA-12908-MS. (MOL.19950123.001)

Greenhaus, M.R., and Zablocki, C.J., 1982, A Schlumberger resistivity survey of the Amargosa Desert, southern Nevada: U.S. Geological Survey Open-File Report 82-897, 150 p.

Healey, D.L., and Miller, C.H., 1965, Gravity survey of the Amargosa Desert area of Nevada and California: U.S. Geological Survey Technical Letter NTS-99, 32 p.

International Union of Geodesy and Geophysics, 1971, Geodetic Reference System 1967: International Association of Geodesy Special Publication no. 3, 116 p. (NNA.901127.0202)

Jachens, R.C., and Moring, B.C., 1990, Maps of thickness of Cenozoic deposits and the isostatic residual gravity over basement for Nevada: U.S. Geological Survey Open-File Report 90-404, 15 p., 2 plates, scale 1:1,000,000.

Kane, M.F., and Bracken, R.E., 1983, Aeromagnetic map of Yucca Mountain and surrounding regions, southwest Nevada: U.S. Geological Survey Open-File Report 83-616, 19 p., 1 plate.

Langenheim, V.E., Carle, S.F., Ponce, D.A., and Phillips, J.D., 1991, Revision of an aeromagnetic survey of the Lathrop Wells area, Nevada: U.S. Geological Survey Open-File Report 91-46, 12 p., 6 fig., 3 plates, 1 magnetic tape.

Langenheim, V.E., Kirchoff-Stein, K.S., and Oliver, H.W., 1993, Magnetic investigations of buried volcanic centers near Yucca Mountain, Nevada: American Nuclear Society Proceedings of the Fourth Annual International Conference on High-Level Waste Management, v. 2, p. 1840-6.

Langenheim, V.E., and Ponce, D.A., 1993, Volume of buried volcanic centers near Yucca Mountain, southwest Nevada, as calculated from aeromagnetic data: American Geophysical Union, v. 74, no. 43, p. 223.

Langenheim, V.E., and Ponce, D.A., 1995, Depth to pre-Cenozoic basement in southwest Nevada: Proceedings, 6th Annual International High-Level Radioactive Waste Management Conference, American Nuclear Society, 3 p.

McElhinny, M.W., 1973, Palaeomagnetism and plate tectonics: Cambridge, Great Britain, Cambridge University Press, 358 p.

Mooney, W.D., and Schapper, S.G., 1995, Seismic refractions studies *in* Oliver, H.W., Ponce, D.A., and Hunter, W. Clay, eds., U.S. Geological Survey Open-File Report 95-74, variously paged.

Morelli, C.(Ed.), 1974, The International Gravity Standardization Net, 1971: International Association of Geodesy Special Publication no. 4, 194 p. (NNA.901127.0203)

Plouff, Donald, 1977, Preliminary documentation for a FORTRAN program to compute gravity terrain corrections based on topography digitized on a geographic grid: U.S. Geological Survey Open-File Report 77-535, 45 p. (NNA.901127.0204)

Ponce, D.A., and Oliver, H.W., 1981, Charleston Peak gravity calibration loop, Nevada: U.S. Geological Survey Open-File Report 81-895, 20 p. (HQS.880517.2827)

Ponce, D.A., Langenheim, V.E., and Sikora, R.F., 1993, Gravity and magnetic data of Midway Valley, southwest Nevada: U.S. Geological Survey Open-File Report 93-540-A, 7 p. (NNA.940418.0157)

Rosenbaum, J.G., and Snyder, D.B., 1985, Preliminary interpretation of paleomagnetic and magnetic property data from drill holes USW G-1, G-2, G-3, and VH-1 and surface localities in the vicinity of Yucca Mountain, Nye County, Nevada: U.S. Geological Survey Open-File Report 85-49, 73 p.

Sawyer, D.A., Fleck, R.J., Lanphere, M.A., Warren, R.G., Broxton, D.E., and Hudson, M.R., 1994, Episodic caldera volcanism in the Miocene southwestern Nevada volcanic field: Revised stratigraphic framework, $^{40}Ar/^{39}Ar$ geochronology, and implications for magmatism and extension: Geological Society of America Bulletin, v. 106, p. 1304-1318.

Snyder, D.B., and Carr, W.J., 1984, Interpretation of gravity data in a complex volcano-tectonic setting, southwest Nevada: Journal of Geophysical Research, v. 89, p. 10,193-10,206.

Swadley, W.C., 1983, Map showing the surficial geology of the Lathrop Wells quadrangle, Nye County, Nevada: U.S. Geological Survey Miscellaneous Investigations Map I-1361, scale 1:48,000.

Swick, C.A., 1942, Pendulum gravity measurements and isostatic reductions: U.S. Coast and Geodetic Survey Special Publication 232, 82 p. (NNA.901204.0008)

U.S. Geological Survey, 1978, Aeromagnetic map of Lathrop Wells area, Nevada: U.S. Geological Survey Open-File Report 78-1103, 3 sheets, scale 1:62,500.

U.S. Geological Survey, 1979, Aeromagnetic map of the Timber Mountain area, Nevada: U.S. Geological Survey Open-File Report 79-587, scale 1:62,500.

Walker, G.E., and Eakin, T.E., 1963, Geology and ground water of Amargosa Desert, Nevada-California: State of Nevada Department of Conservation

and Natural Resources Ground Water Resources-Reconnaissance Series Report 14, 45 p., 4 plates.

Wright, L.A., 1989, Overview of the role of strike-slip and normal faulting in the Neogene history of the region northeast of Death Valley, California-Nevada: Nevada Bureau of Mines and Geology Open-File 89-1, p. 1-11.
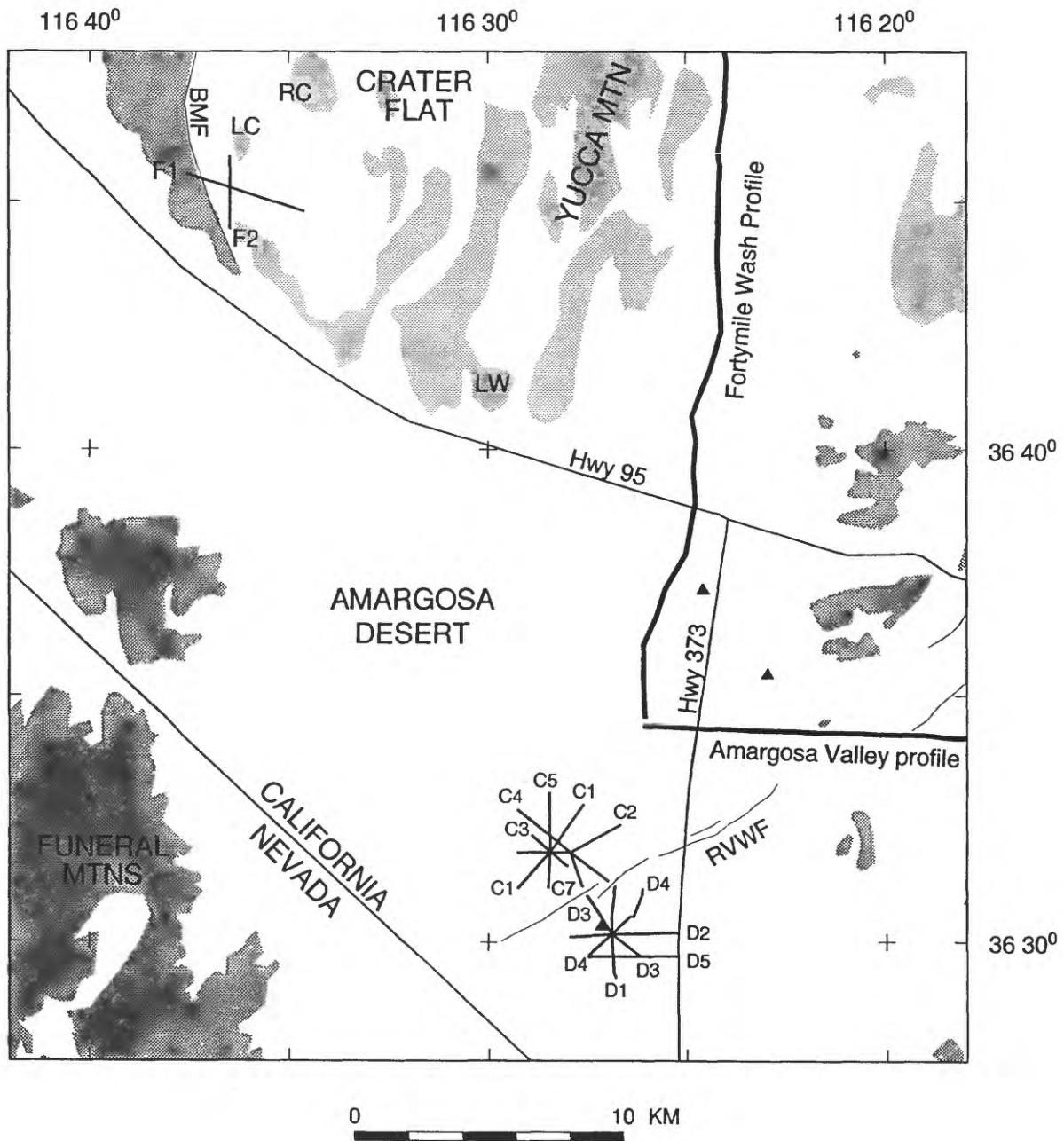
Figure 1. Map of study area. Lightly shaded regions denote outcrops of Tertiary and Quaternary volcanic rocks; darker areas, Precambrian and Paleozoic sedimentary rocks; white areas, Tertiary and Quaternary alluvium. Filled triangles show locations of drillholes that penetrated basalt. RC, Red Cone, LW, Lathrop Wells volcanic center, LC, Little Cones, BMF, Bare Mountain fault, RVWF, Rock Valley Wash Fault. Very thick lines are seismic profiles; short thick lines are gravity and magnetic profiles collected over anomalies C, D, and F.
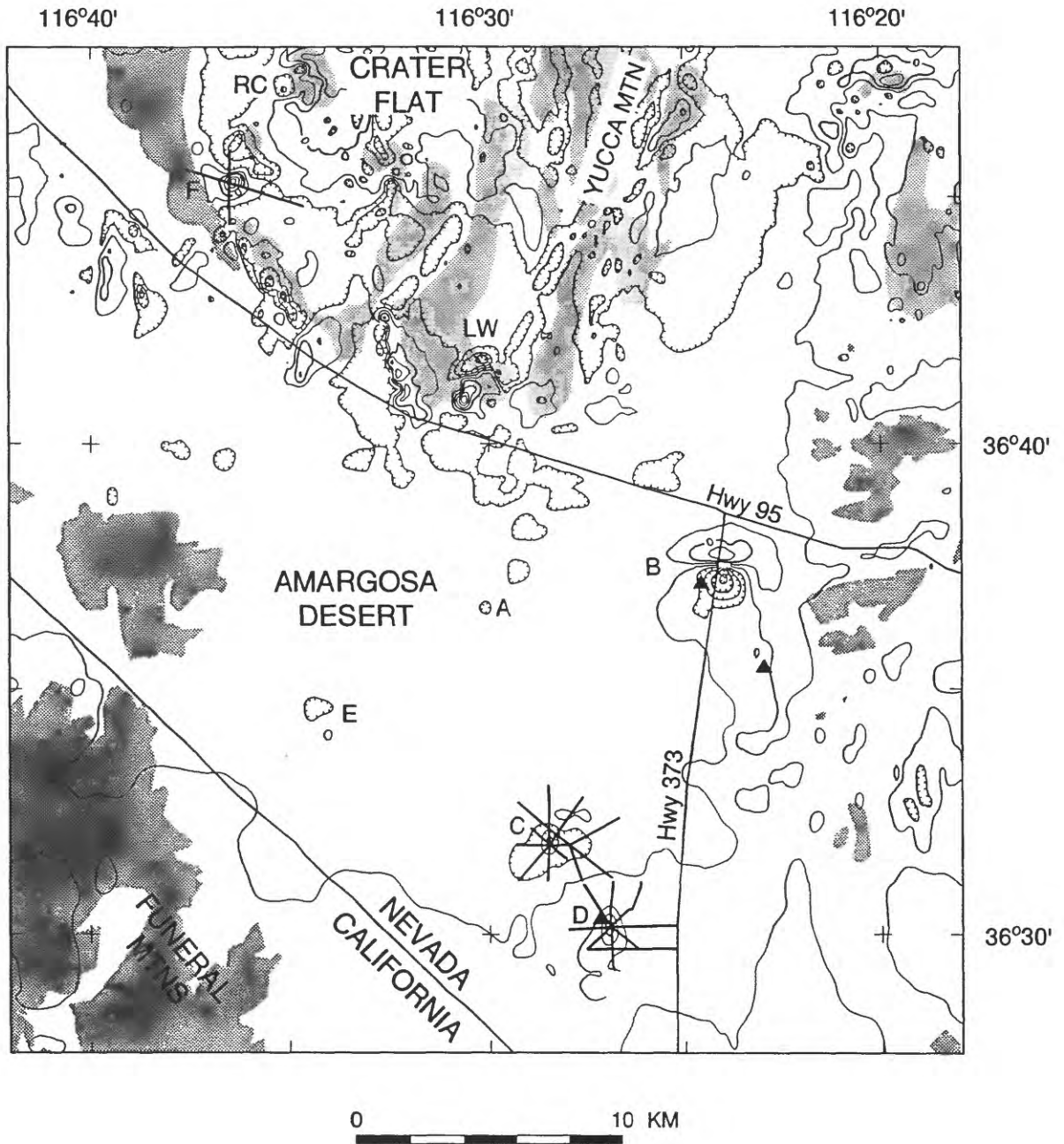
Figure 2. Aeromagnetic map of the Amargosa Desert and Crater Flat region, southwest Nevada. Contour interval 100 nT. Lightly shaded regions denote areas of Tertiary and Quaternary volcanic rocks; darker areas, Precambrian and Paleozoic sedimentary rocks; white areas, Tertiary and Quaternary alluvium. Filled triangles show locations of drillholes that penetrated basalt. Thick lines show locations of detailed geophysical profiles over anomalies C, D, and F. LW and RC refer to the aeromagnetic anomalies associated with the Lathrop Wells and Red Cone volcanic centers.
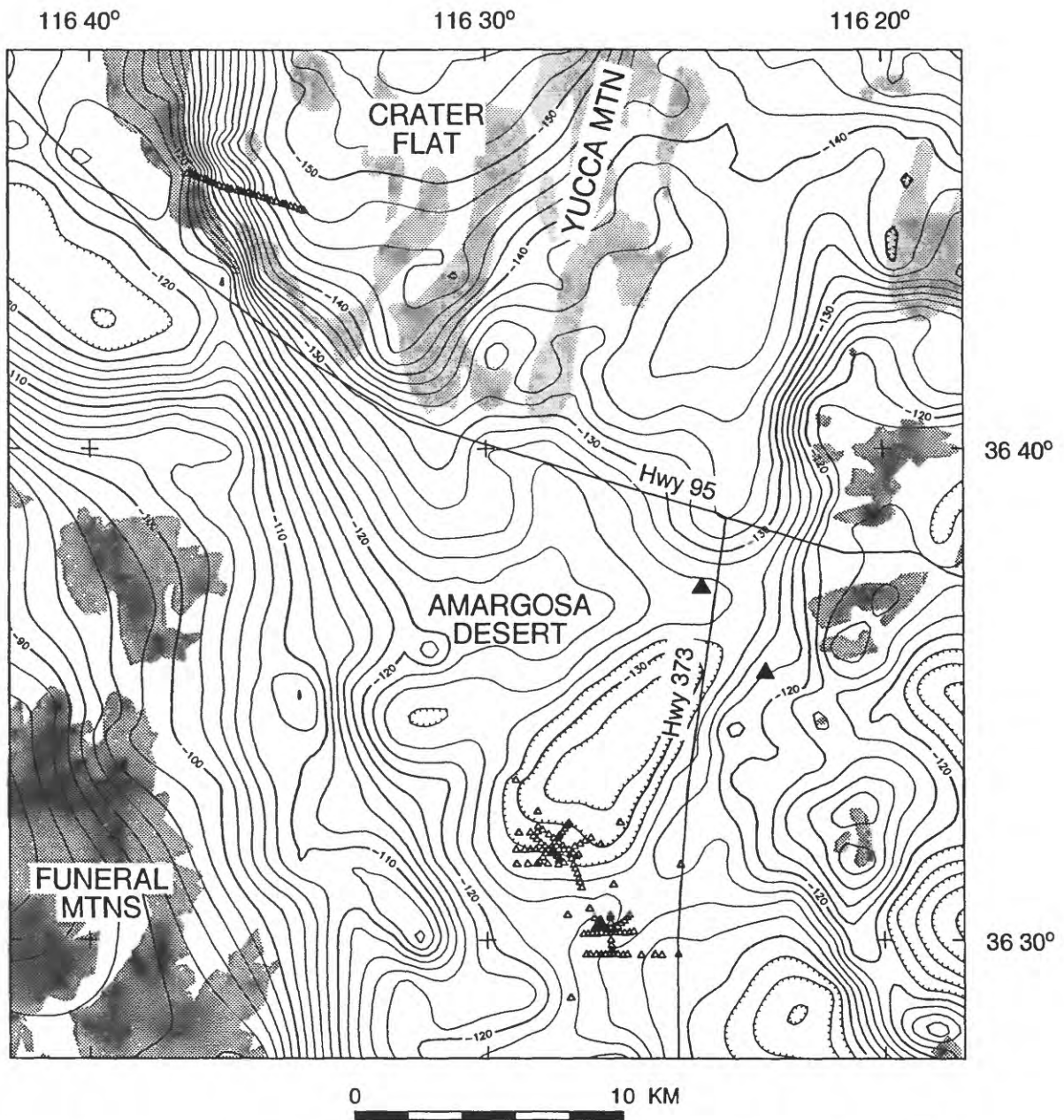
Figure 3. Complete Bouguer gravity map of the Amargosa Desert and Crater Flat region, southwest Nevada. Contour interval 2 mGal. Reduction density 2.67 g/cm³. Lightly shaded regions denote outcrops of Tertiary and Quaternary volcanic rocks; darker areas, Precambrian and Paleozoic sedimentary rocks; white areas, Tertiary and Quaternary alluvium. Filled triangles show locations of drillholes that penetrated basalt. Unfilled triangles show locations of individual gravity stations collected over aeromagnetic anomalies.
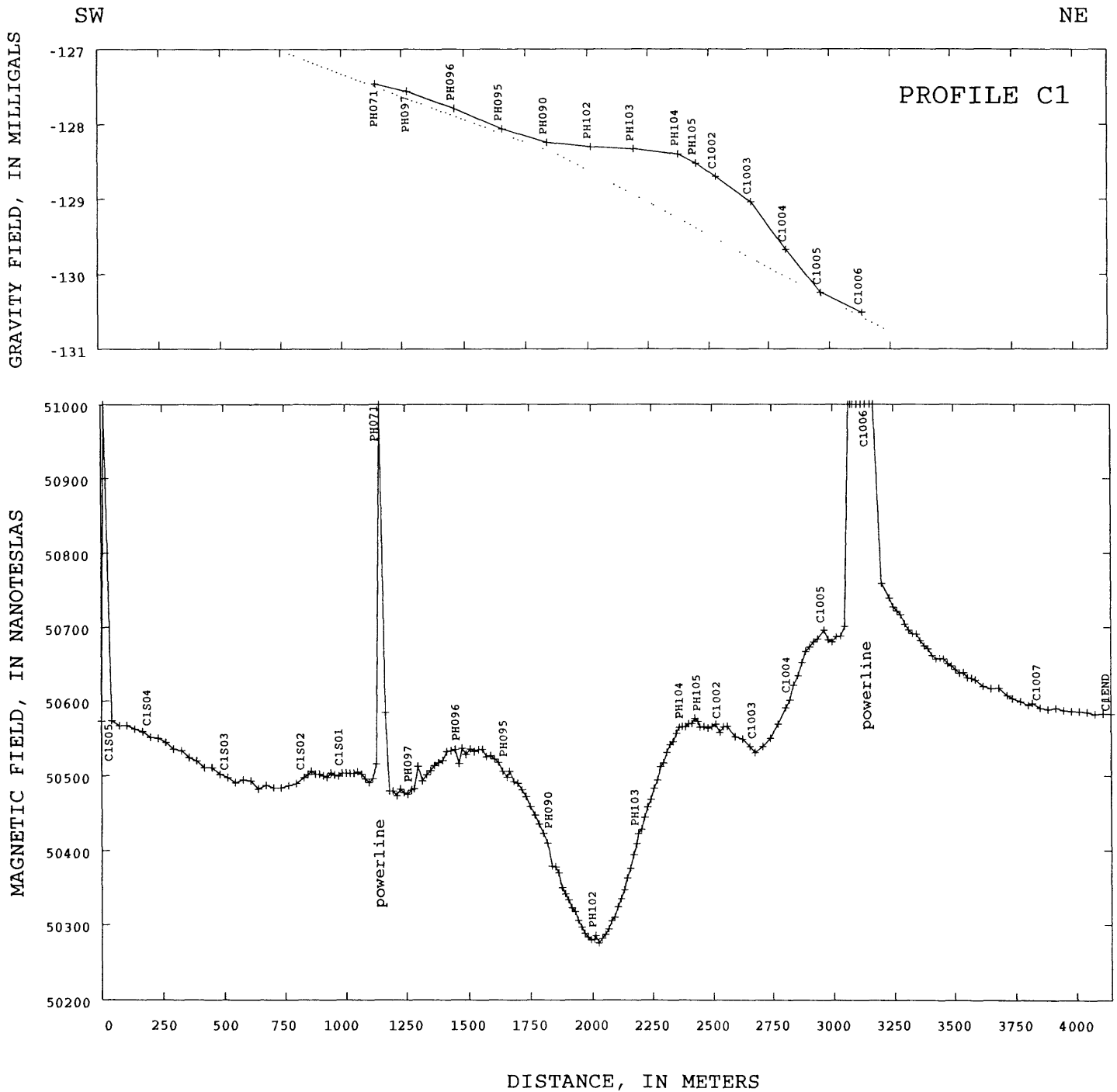
Figure 4a. Complete Bouguer gravity and ground magnetic data along profile C1. Reduction density, 2.67 g/cm^3. Dashed line is regional gravity field as derived from gridded gravity values.
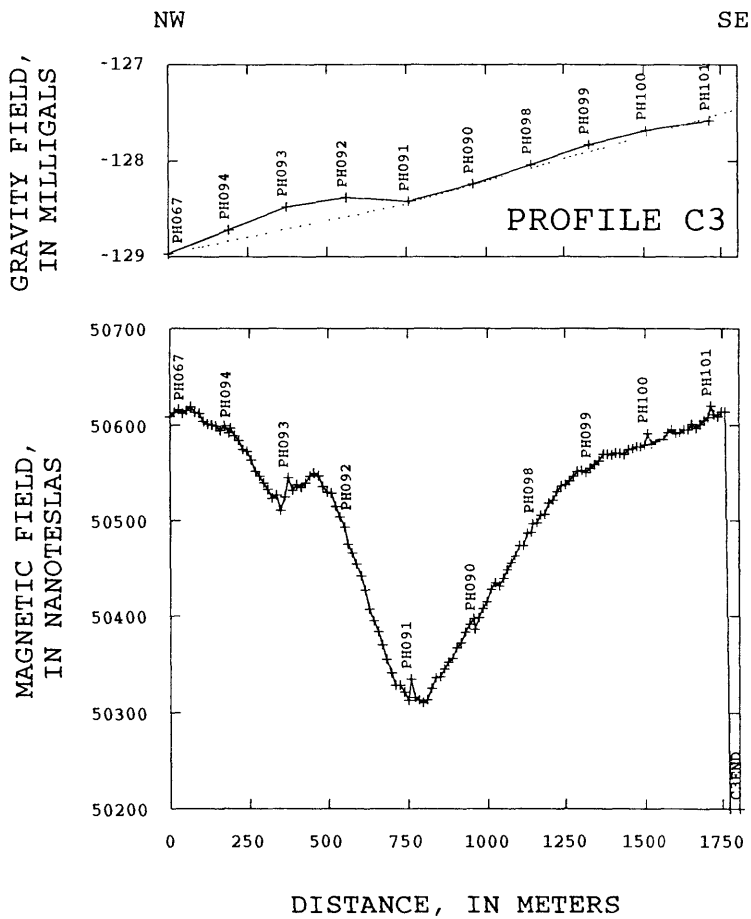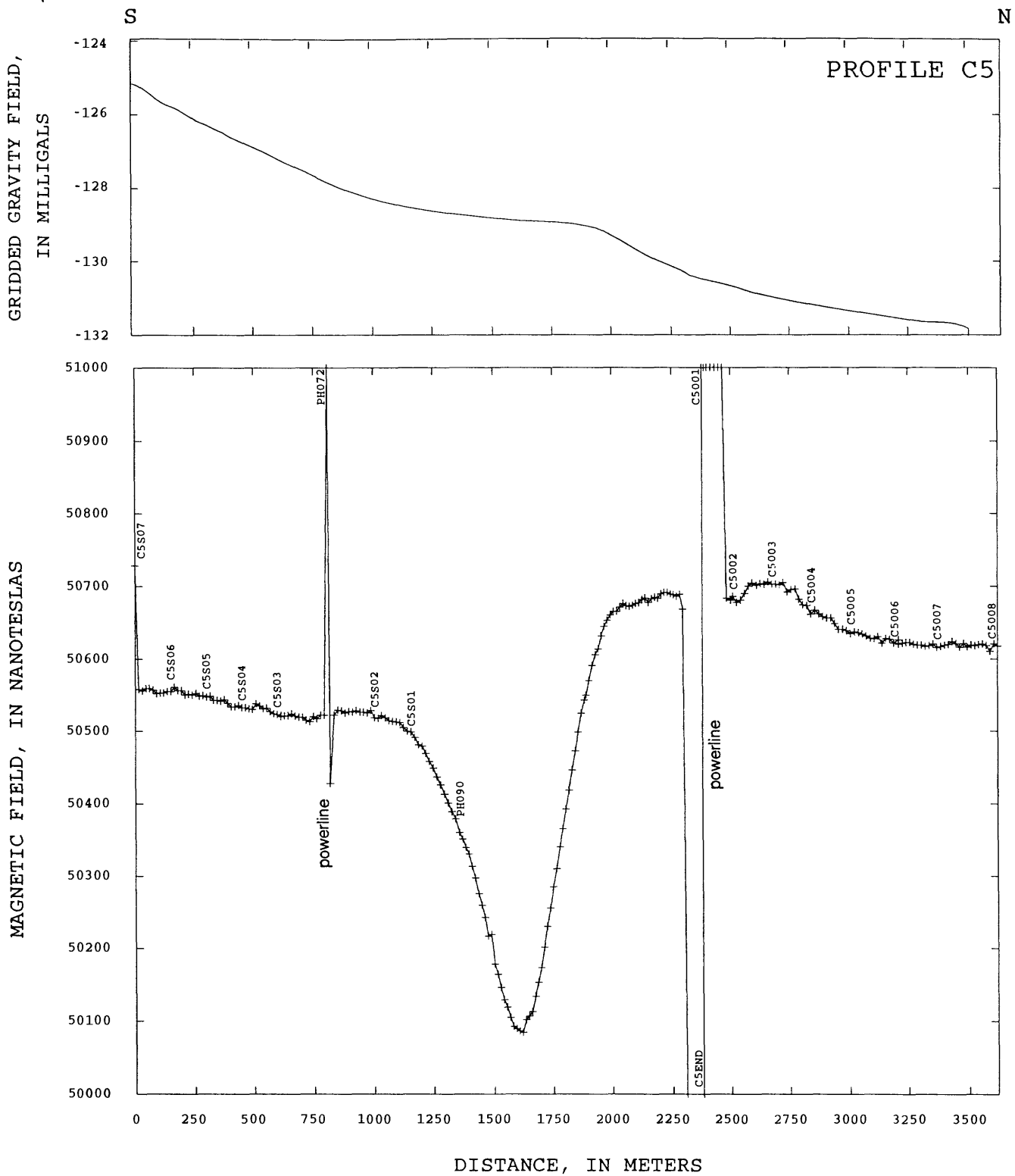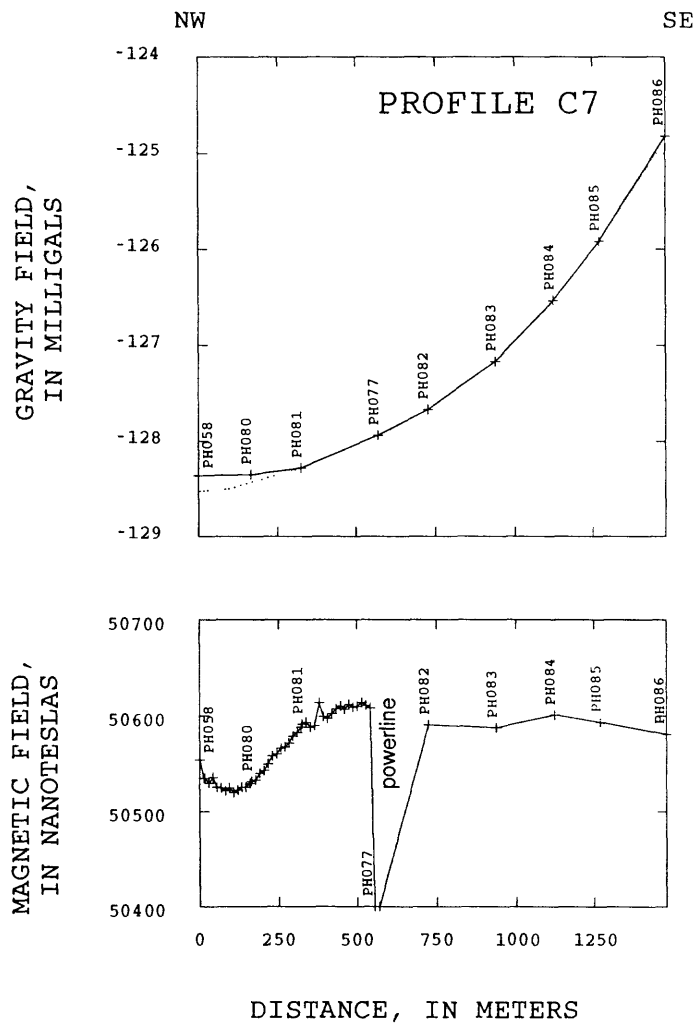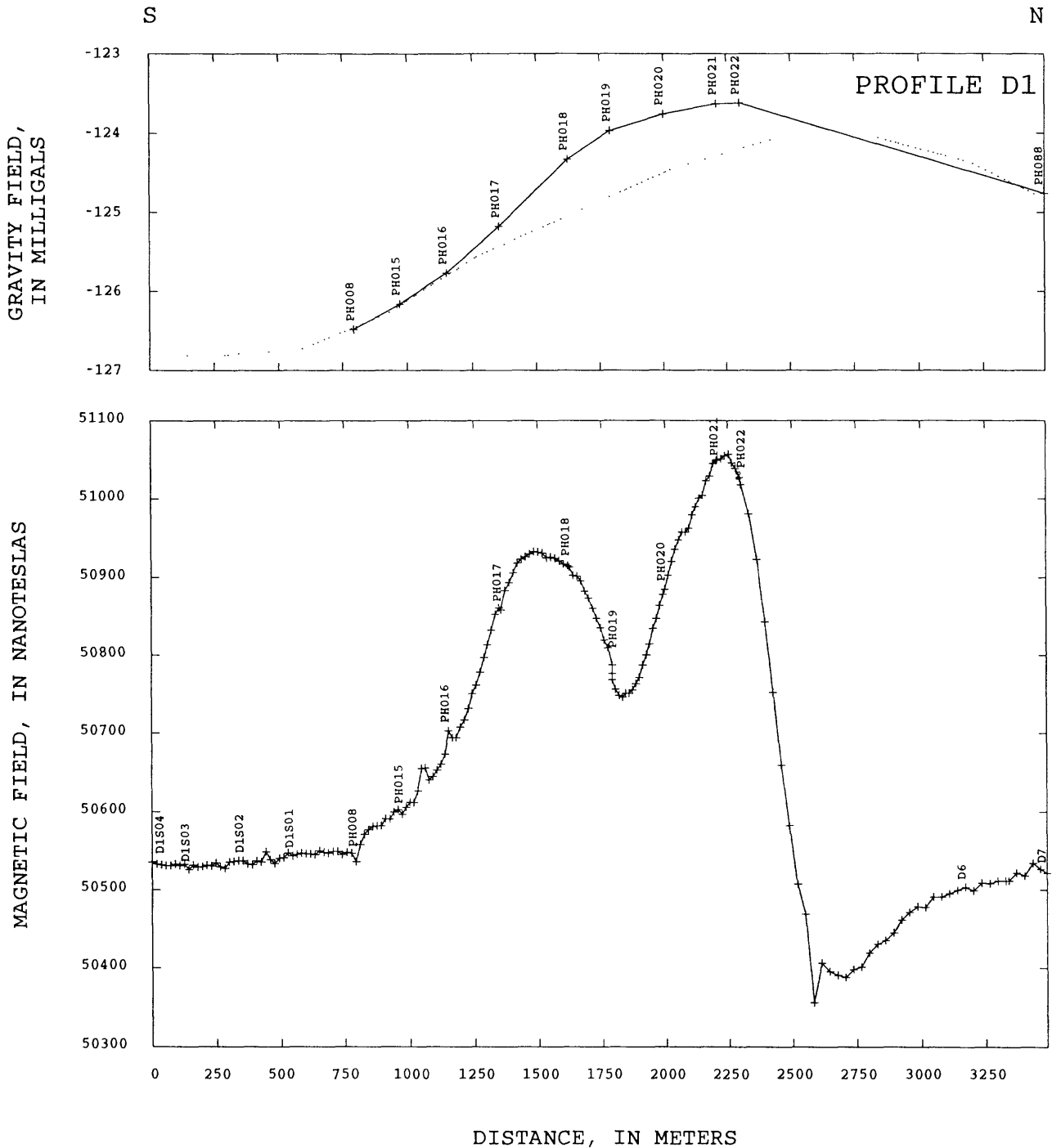
Figure 4c.   Complete Bouguer gravity and ground magnetic data along profile C3.
Reduction density 2.67 g/cm3.   Dashed line is regional gravity
field as derived from gridded gravity values.

MAGNETIC FIELD, IN NANOTESLAS

GRAVITY FIELD, IN MILLIGALS

PROFILE C2

W   E   NE

DISTANCE, IN METERS
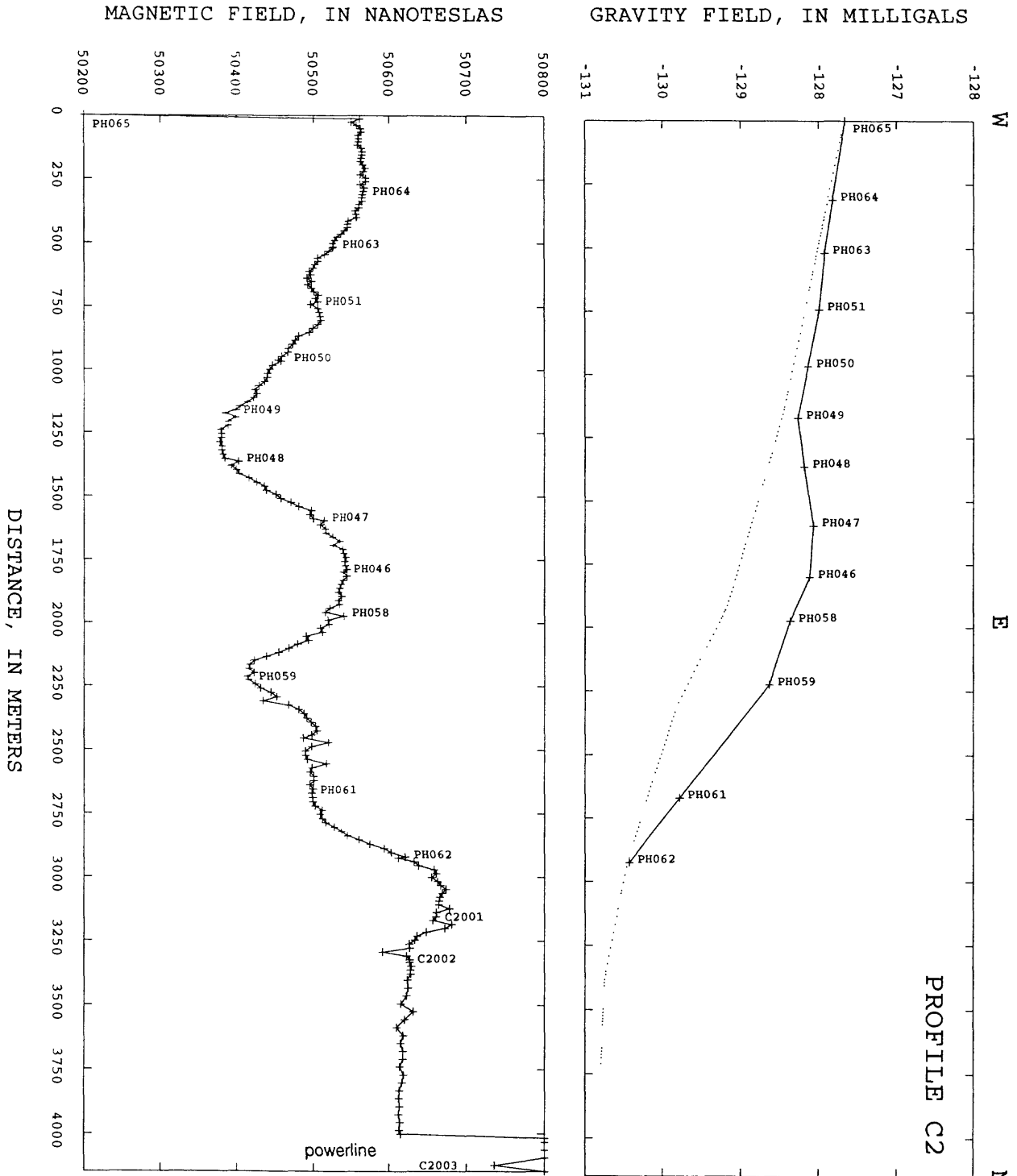
Figure 4b. Complete Bouguer gravity and ground magnetic data along profile C2.
Reduction density, 2.67 g/cm³. Dashed line is regional gravity field
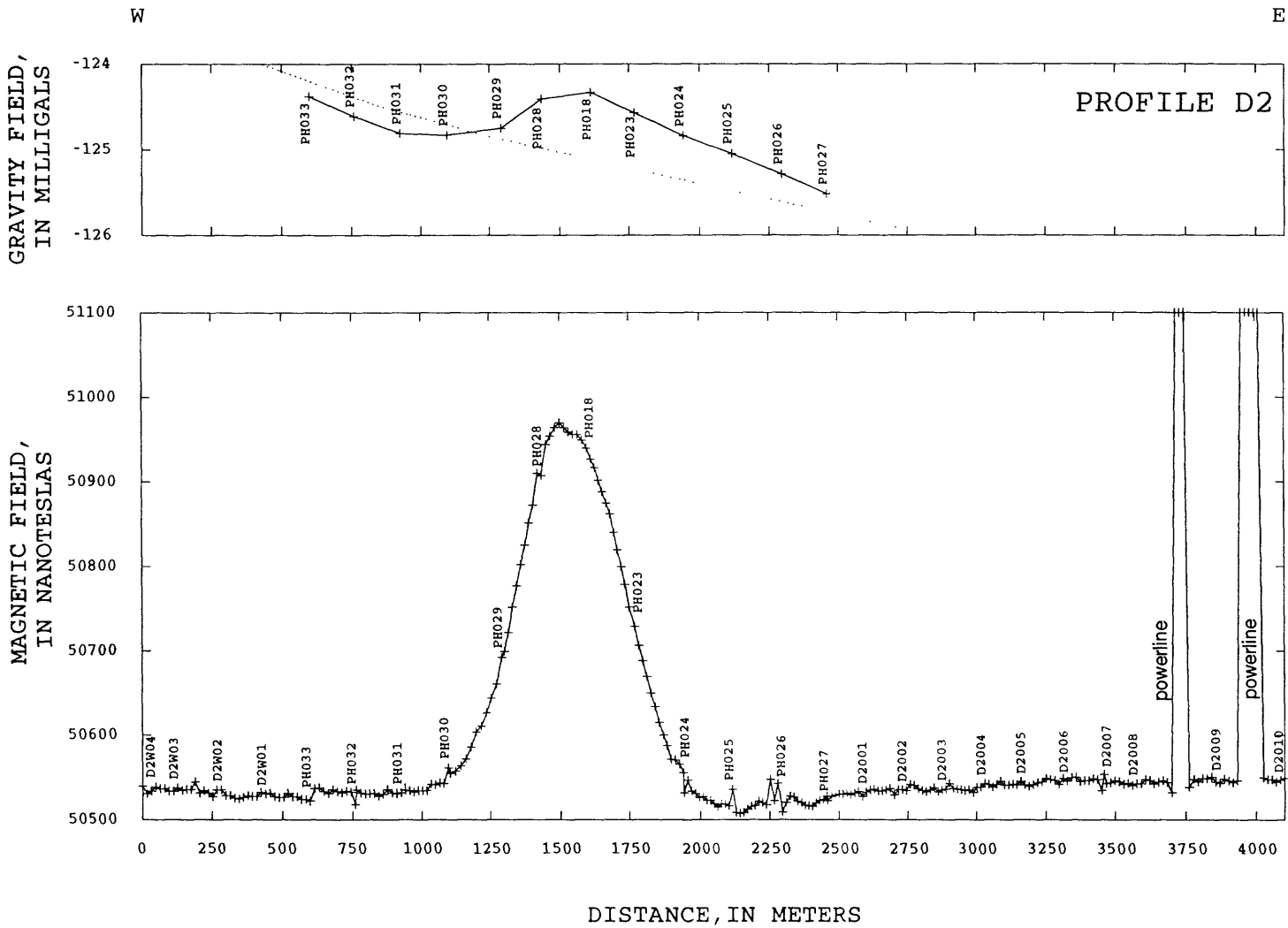as derived from gridded gravity values.

23
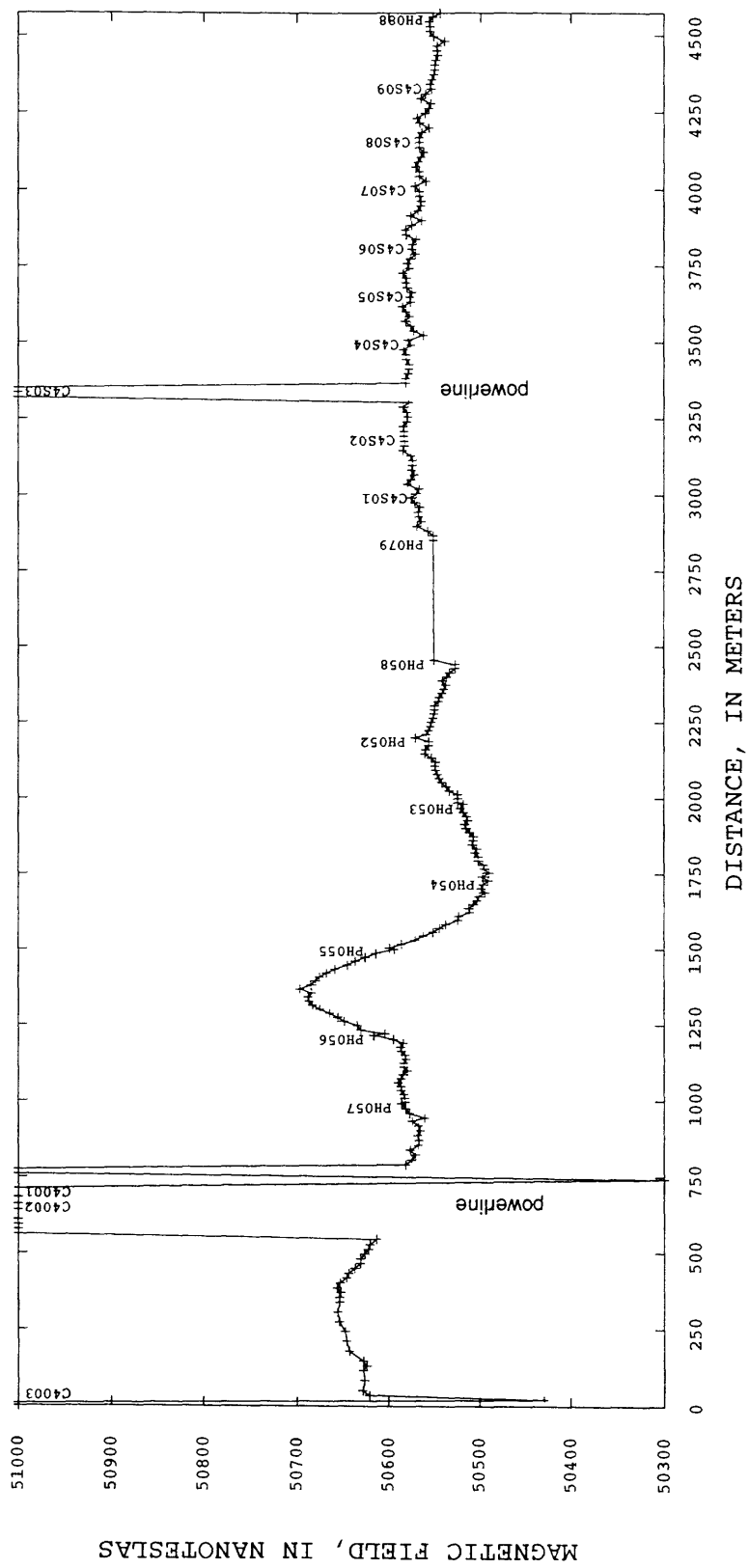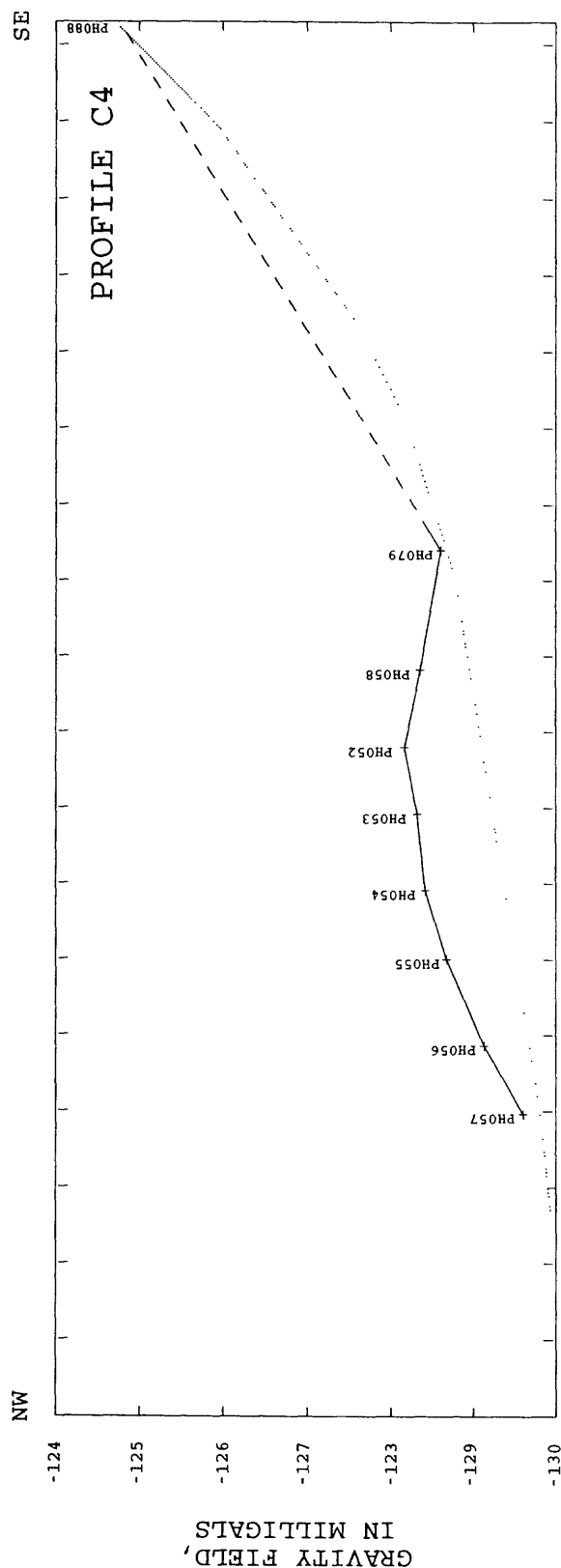
Figure 4d. Complete Bouguer gravity and ground magnetic data along profile C4. Reduction density of 2.67 g/cm3. Dashed gray line is regional gravity field as derived from gridded gravity data.

24

Figure 4e.   Ground magnetic data along profile C5. Gravity derived
from gridded values.

Figure 4f. Complete Bouguer gravity and ground magnetic data along profile C7. Reduction density of 2.67 g/cm^3. Dashed line is regional gravity field as derived from gridded gravity data.
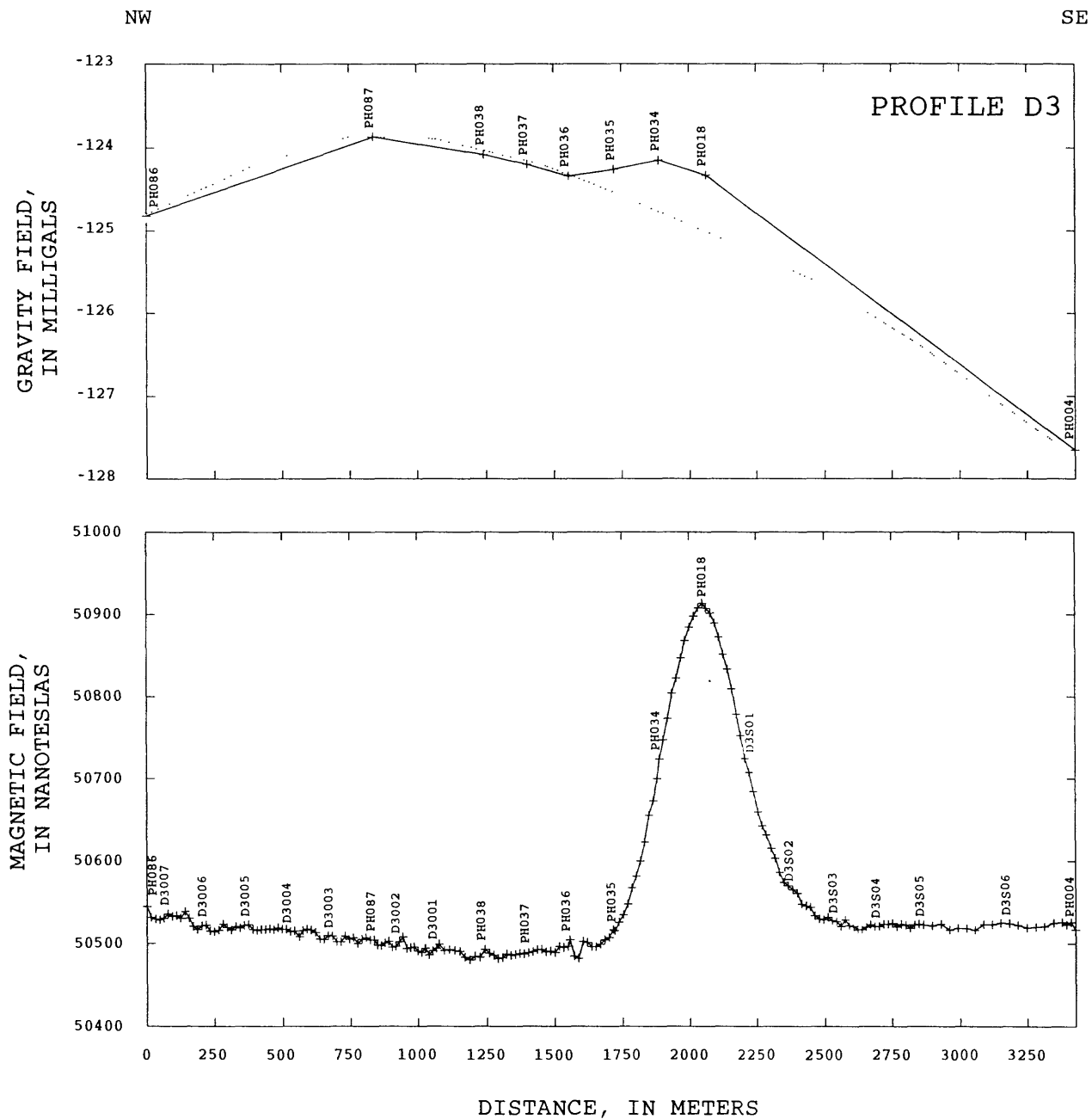
Figure 5a. Complete Bouguer gravity and ground magnetic data along profile D1. Reduction density, 2.67 g/cm^3. Dashed line is regional gravity field as derived from gridded gravity data.
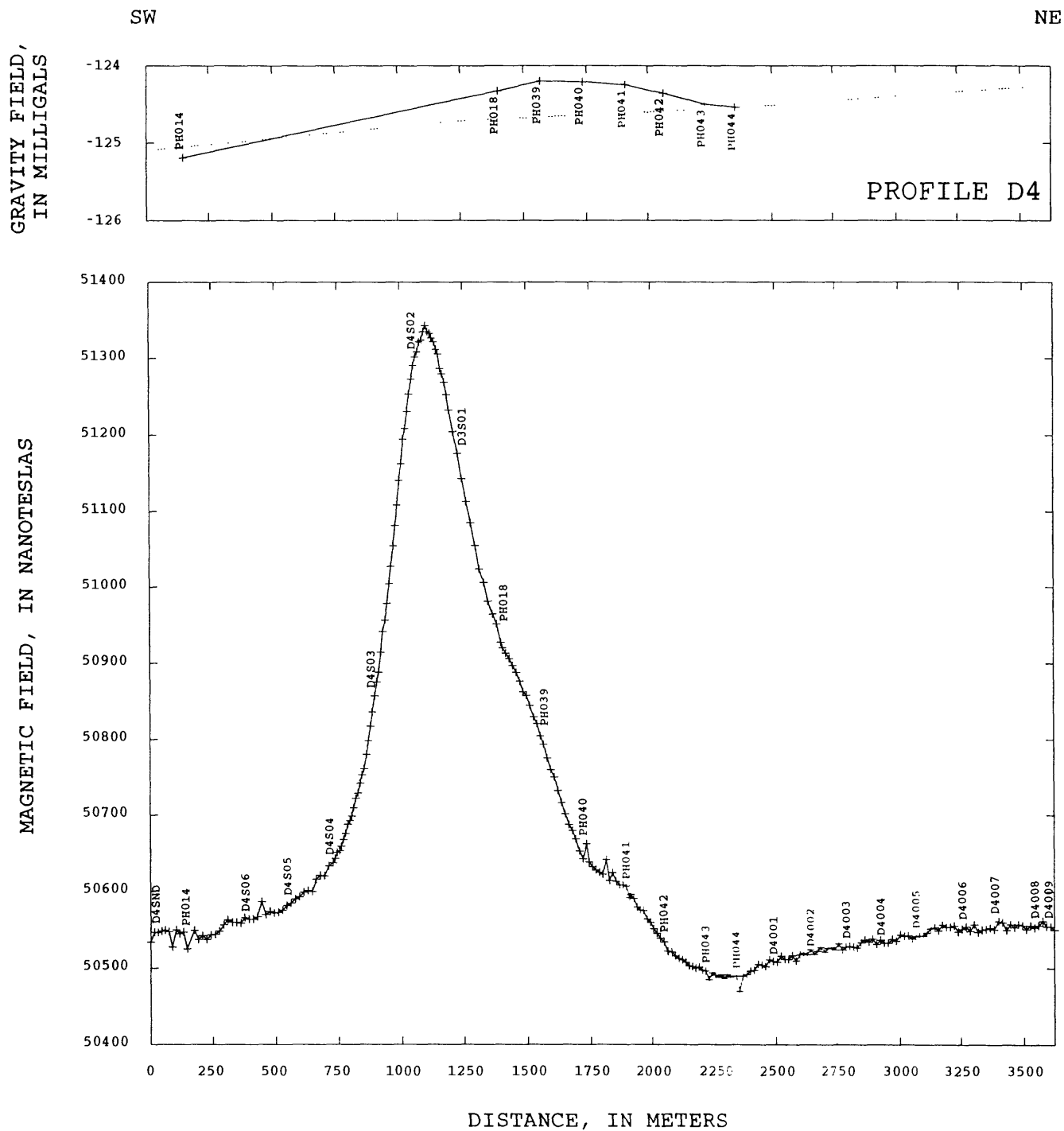
Figure 5b. Complete Bouguer gravity and ground magnetic data along D2.
Reduction density, 2.67 g/cm³. Dashed line is regional gravity field
as derived from gridded gravity data.

Figure 5c. Complete Bouguer gravity and ground magnetic data along profile
D3. Reduction density, 2.67 g/cm^3. Dashed line is regional gravity
field as derived from gridded gravity data.

29

Figure 5d. Complete Bouguer gravity and ground magnetic data along profile D4.
Reduction density, 2.67 g/cm3. Dashed line is regional gravity field
as derived from gridded gravity data.

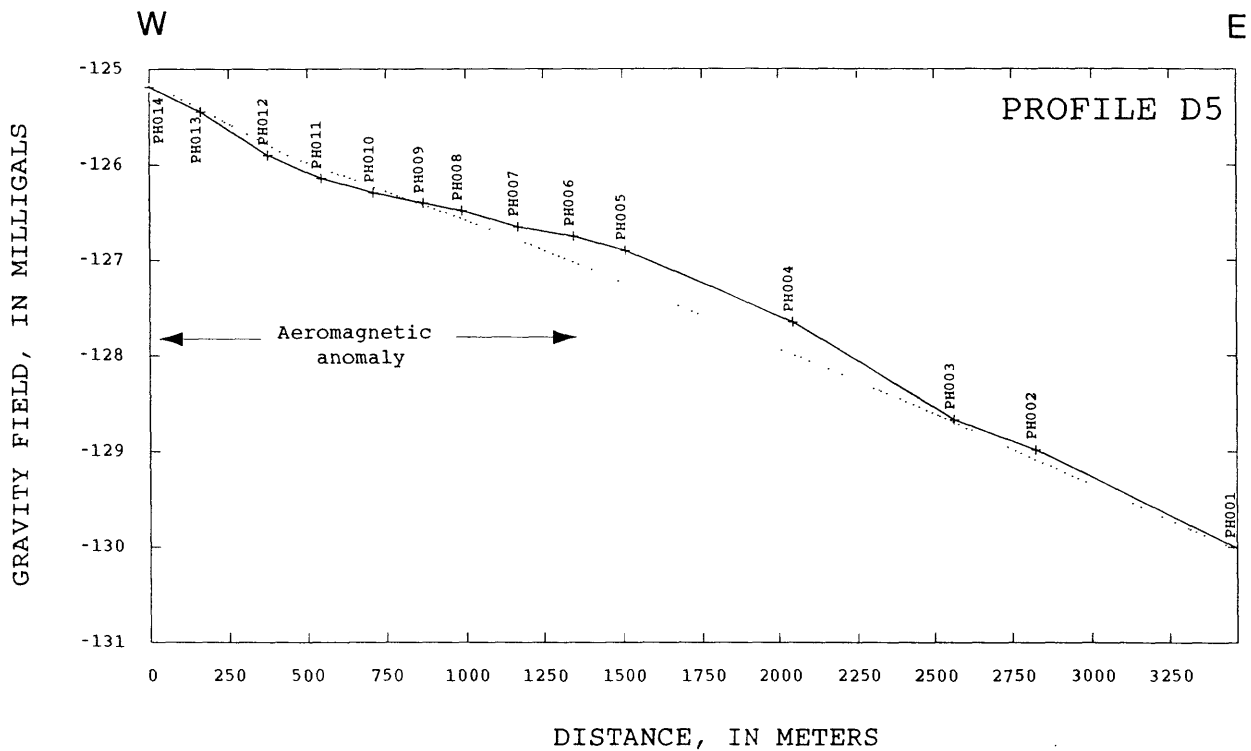30

W   E

PROFILE D5

GRAVITY FIELD, IN MILLIGALS

Aeromagnetic
anomaly

DISTANCE, IN METERS

Figure 5e. Complete Bouguer gravity data along profile D5. Reduction density, 2.67 g/cm^3. Ground magnetic data were not collected because of profile's proximity to powerline. Dashed line is regional gravity field as derived from gridded gravity data.
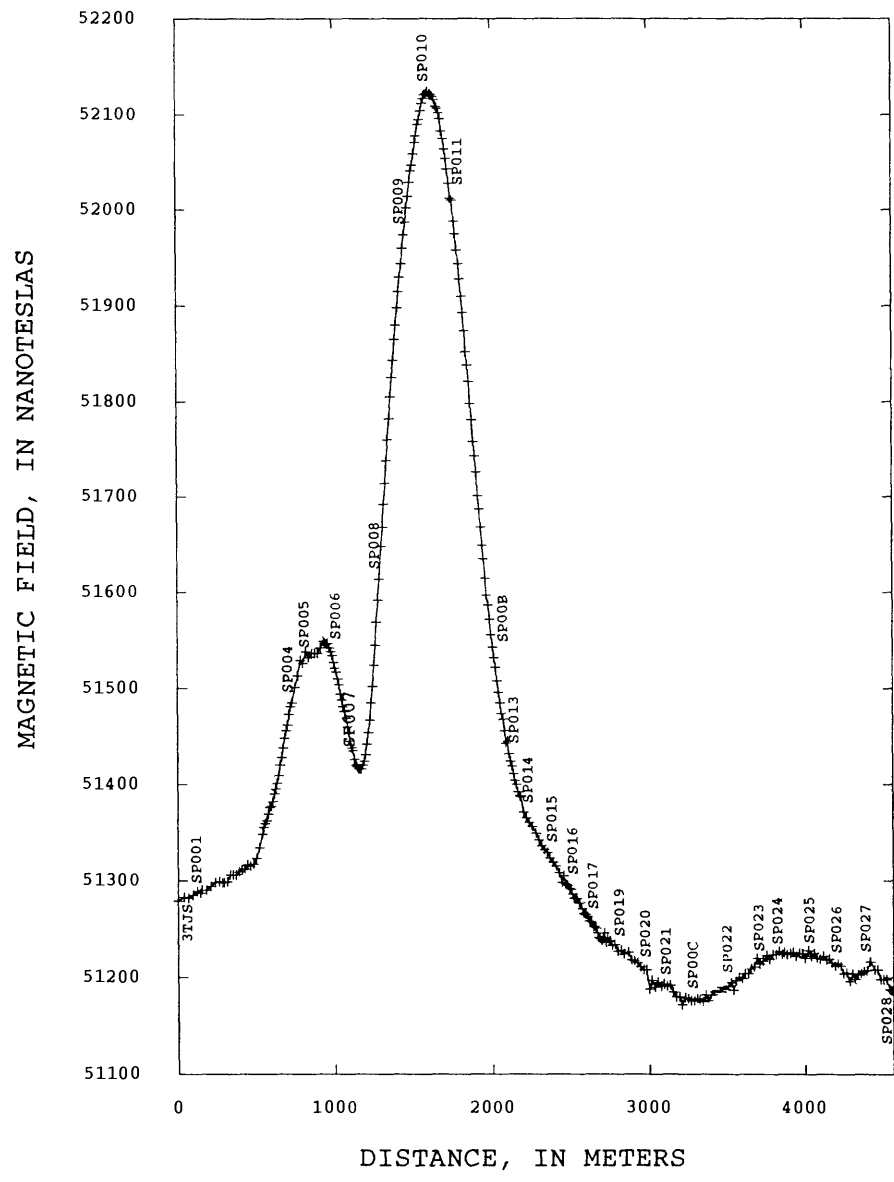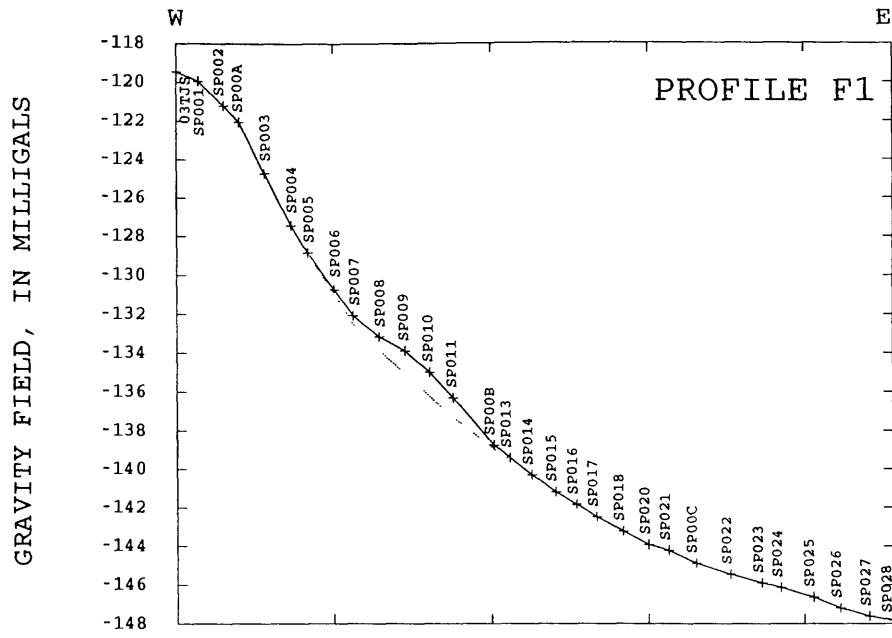
Figure 6a. Ground magnetic and complete Bouguer gravity data along profile F1.
Reduction density, 2.67 g/cm3. Dashed line is regional gravity field
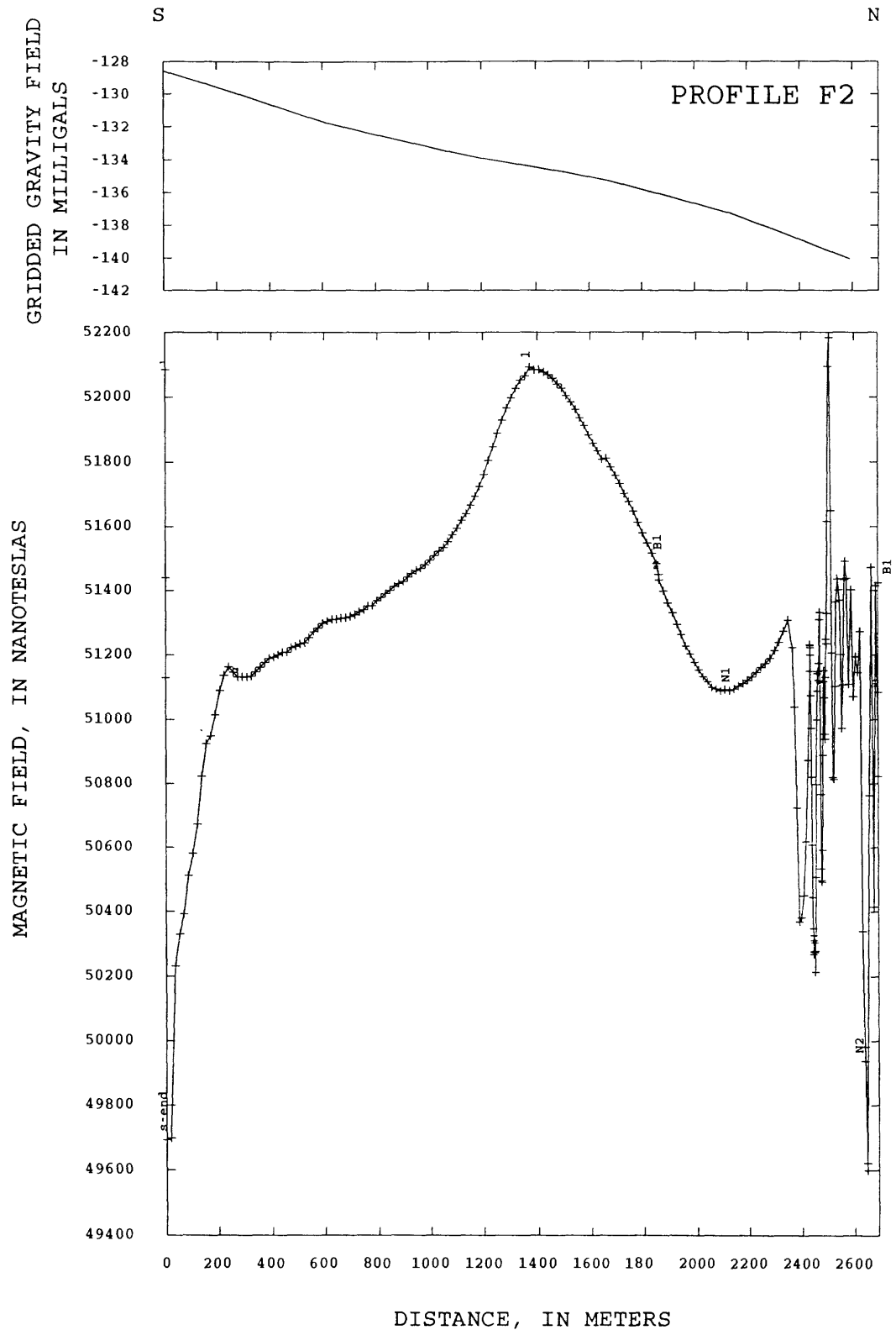as derived from gridded gravity data.

Figure 6b. Ground magnetic data along profile F2. Gravity values taken
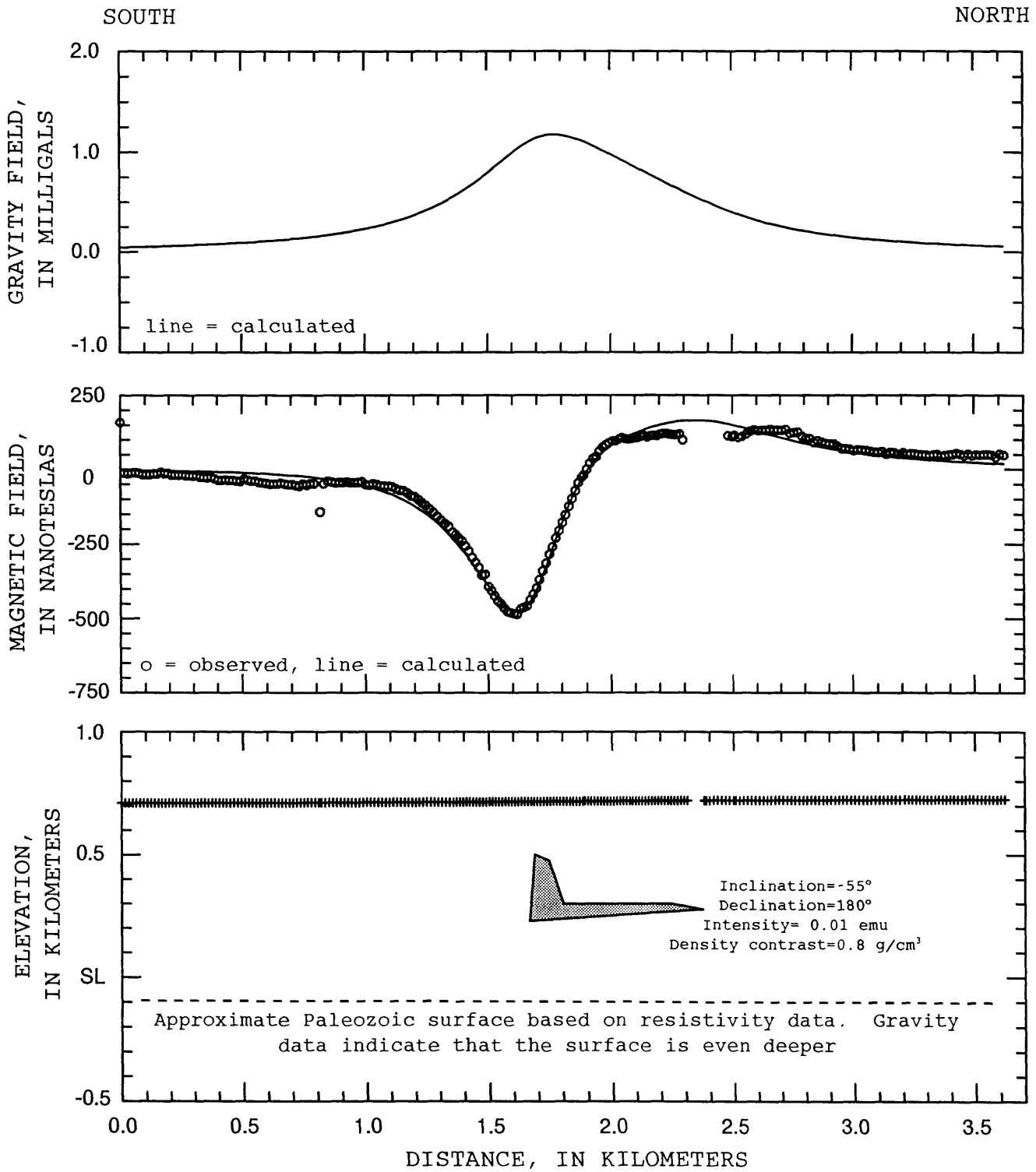from grid.

Figure 7. 2-1/2-dimensional model of profile C5.

The figure contains three stacked plots sharing the x-axis "DISTANCE, IN KILOMETERS" (0.0 to 3.5), with "SOUTH" labeled at top left and "NORTH" at top right.

Top plot — y-axis "GRAVITY FIELD, IN MILLIGALS" (-1.0 to 2.0):
line = calculated

Middle plot — y-axis "MAGNETIC FIELD, IN NANOTESLAS" (-750 to 250):
o = observed, line = calculated

Bottom plot — y-axis "ELEVATION, IN KILOMETERS" (-0.5 to 1.0, with SL marked):
Inclination=-55°
Declination=180°
Intensity= 0.01 emu
Density contrast=0.8 g/cm³

Approximate Paleozoic surface based on resistivity data. Gravity data indicate that the surface is even deeper
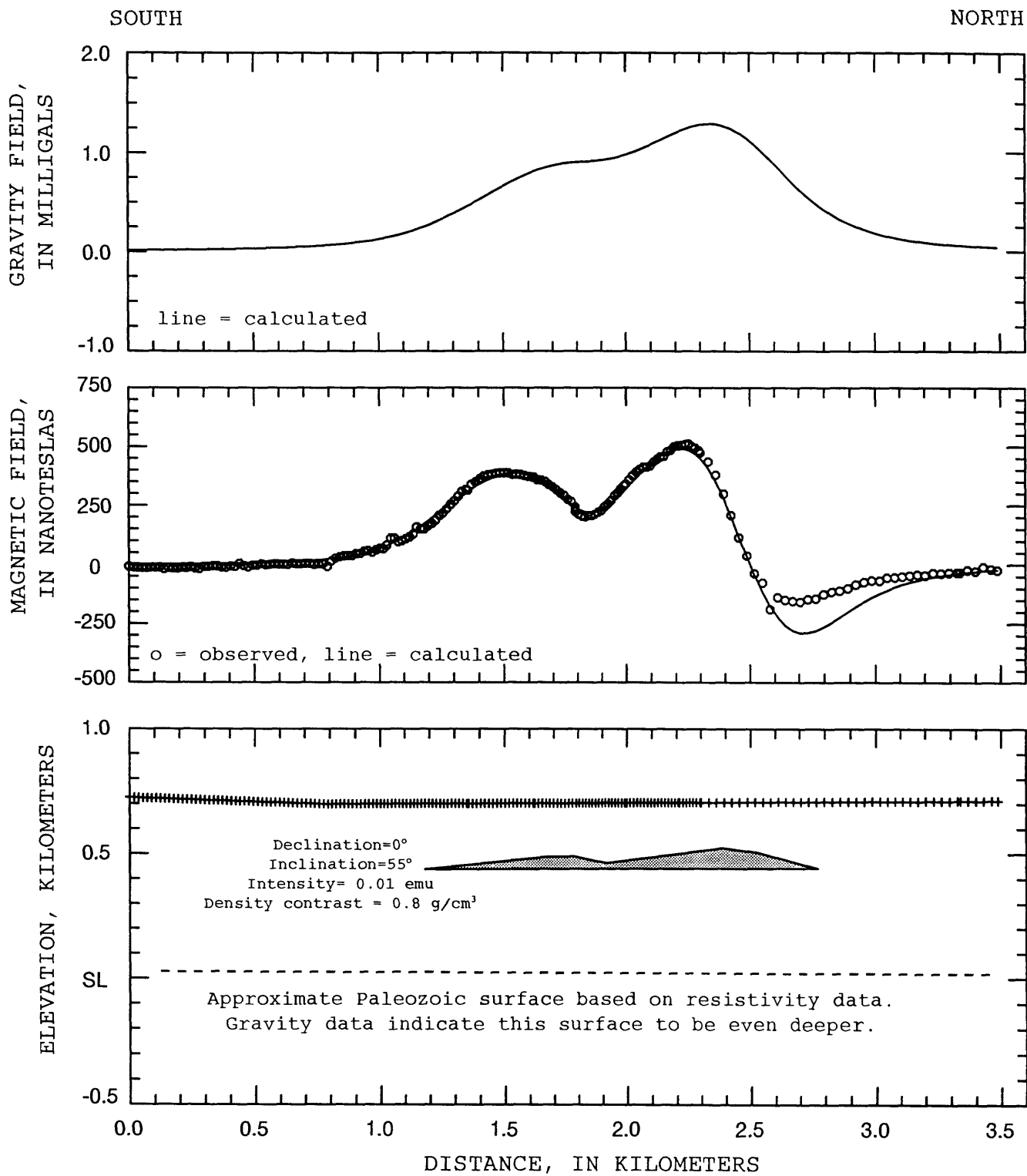
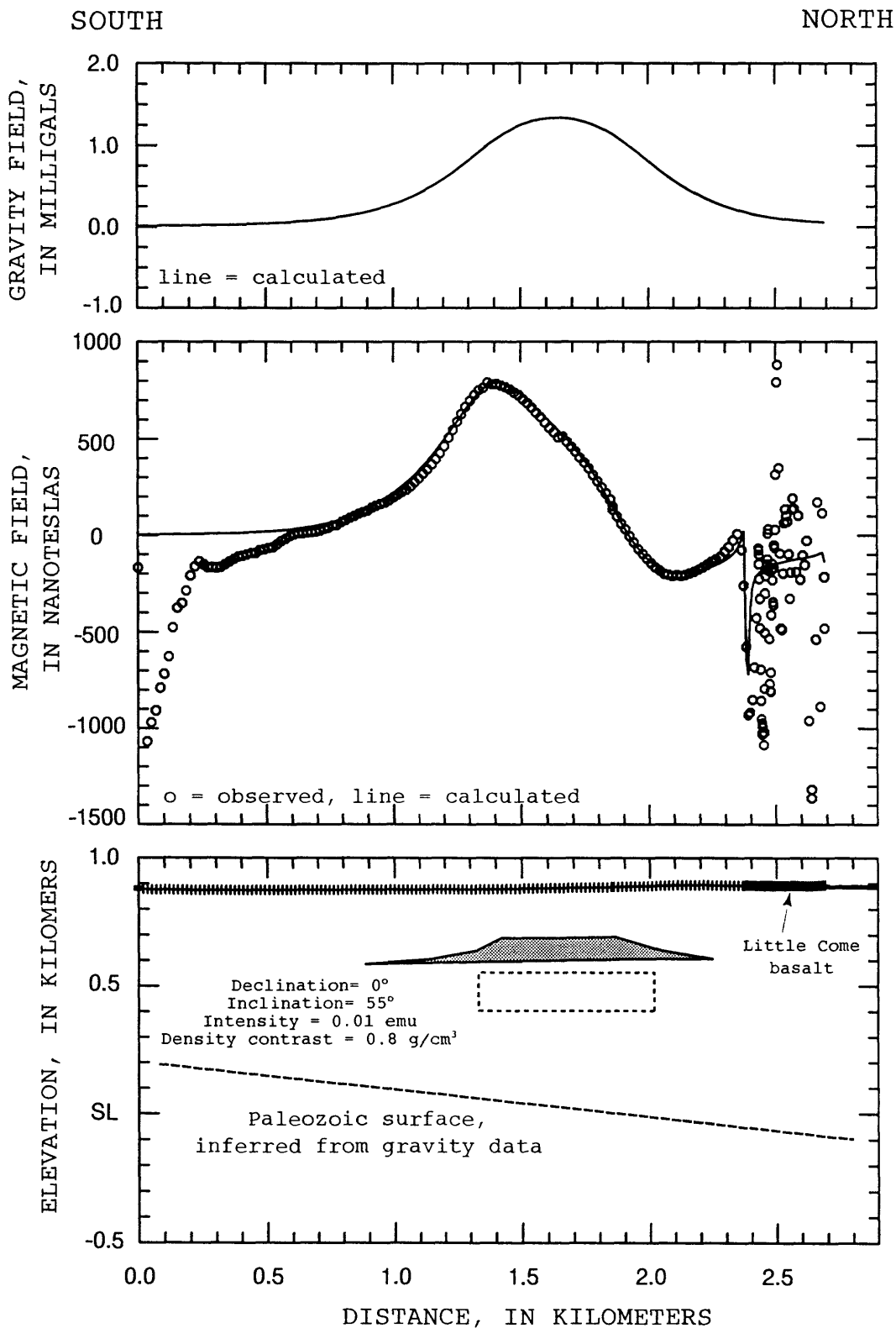Figure 8. 2-1/2-dimensional modeling along profile D1.

Figure 9. 2-1/2-dimensional modeling along profile F2. Dashed body gives same
calculated magnetic field curve as the shaded body, but gives estimate
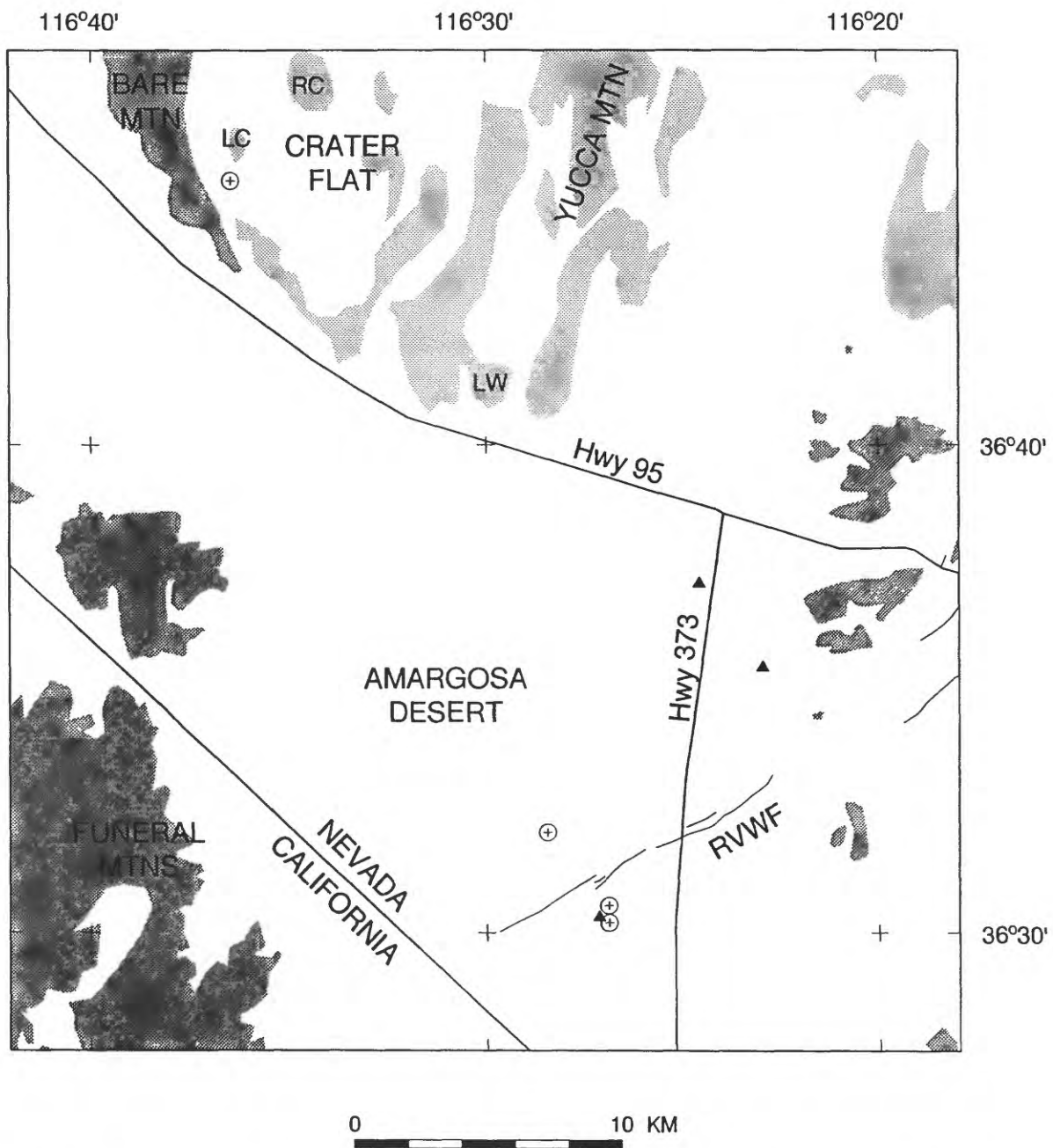of the maximum depth to the top of the causative body.

Figure 10. Map showing the locations of proposed drilling locations based on magnetic modeling. Abbreviations same as in Figure 1. Lightly shaded regions denote outcrops of Tertiary and Quaternary volcanic rocks; darker areas, Precambrian and Paleozoic sedimentary rocks; white areas, Tertiary and Quaternary alluvium. Filled triangles show locations of drillholes that penetrated basalt. Circles with crosses show locations of proposed drilling locations based on magnetic modeling.